

**ATOMIC FORCE MICROSCOPY OF THE INTERVESSEL  
PIT MEMBRANE IN THE STEM OF *SAPIUM SEBIFERUM*  
(EUPHORBIACEAE)**

**Thomas C. Pesacreta<sup>1</sup>, Leslie H. Groom<sup>2</sup> & Timothy G. Rials<sup>2</sup>**

**SUMMARY**

Sapwood and juvenile wood of *Sapium sebiferum* (Euphorbiaceae) was collected during 2000–2002. In air-dried vessel elements, the surface of pit membranes (PMs) in the outermost growth ring was coated with plaque-like or interstitial material that was 2–5 nm thick. This coating was phase dark and overlaid a phase bright layer of globules and reticulately arranged microfibrils (MFs) that was 25–50 nm thick. Beneath the reticulate layer there was another surface exposed during sectioning/fracturing. It had parallel MFs which appeared to be continuous with the middle lamella, and were also coated. The total thickness of the dried PM appeared to be in the range of 50–100 nm. Overwintering and heartwood PMs were encrusted with a non-microfibrillar layer that differed from the above mentioned coating. Prior to chemical treatment, specific dried, untreated PMs were located and then the sample was dismounted, treated with acidic H<sub>2</sub>O<sub>2</sub>, and observed after treatment so that before and after images could be compared. Treatment with acidic H<sub>2</sub>O<sub>2</sub> removed some of the coating and greatly modified the fibrillar nature of the surface layer, but did not reduce its overall thickness. The native structure of sapwood PMs was observed in water. Non-dried PMs displayed two layers, each with a different type of surface. The outer layer was non-microfibrillar and covered the entire surface of the PM. The non-microfibrillar layer was extremely sensitive to mechanical perturbation by the AFM tip, and had phase characteristics similar to the coating of dried PMs. The underlying layer was thick and microfibrillar. The MFs in non-dried PMs were, like the dried MFs, phase bright but they were much more loosely intermeshed compared with those seen in dried materials. The measurable thickness (which does not represent the total thickness) of non-dried PMs frequently ranged from 90–225 nm, although a few 500 nm vertical features were measured.

**Key words:** Atomic force microscopy, cellulose microfibril, Euphorbiaceae, pit membrane, *Sapium*, transpiration, vessel, wood structure, xylem.

- 1) University of Louisiana at Lafayette, Microscopy Center, P.O. Box 42451, Lafayette, LA 70504, U.S.A.; corresponding author.
- 2) USDA, Forest Service, Southern Research Station, 2500 Shreveport Highway, Pineville, LA 71360, U.S.A.

## INTRODUCTION

The atomic force microscope (AFM) is a surface scanning instrument. Gerd Binnig and Heinrich Rohrer received the 1986 Nobel Prize in Physics for designing it. During the past decade the AFM has become a widely used scientific tool with resolution capabilities similar to those of electron microscopes (Duchesne & Daniel 1999). This microscope-without-a-lens operates by scanning a sharp tip, mounted on a flexible cantilever, across the surface of a sample. In brief, the vertical displacement of the tip is quantified to determine the height of surface features. From such data it is possible to construct a digitized, 3-dimensional data set that shows ultrastructural features and quantifies roughness. The AFM can also be used to study mechanical properties such as surface hardness or adhesion by analyzing phase changes in the oscillation of the tip as it is rastered across the surface. Operation is possible in either water, air or a vacuum.

Because AFM technique does not require staining, coating, or high vacuum for operation it can be used to study biological materials in their native state. Several purified carbohydrates have been imaged with the AFM including native *Valonia* cellulose (Hanley *et al.* 1992; Kuutti *et al.* 1994; Baker *et al.* 1997), xanthan gums (Kirby *et al.* 1995), bacterial polysaccharides (Kirby *et al.* 1995), pectin (Round *et al.* 1997), lignin-carbohydrates (Shevchenko *et al.* 1998), and dextran (Rief *et al.* 1997). These studies have provided information regarding crystallinity, and helical conformation. Matsumura and Glasser (2000) used AFM phase data to analyze biphasic component distribution related to mechanical properties of synthetic composites. There have been some AFM studies of intact or partially extracted plant cell walls. Kirby *et al.* (1996) examined the wall structure of partially purified cell wall fragments from several species. They analyzed hydrated wall fragments and observed images similar to those produced with the much more technically challenging freeze, deep etch, rotary shadowing methods of Heuser (1981) and McCann *et al.* (1990). Pesacreta *et al.* (1997) imaged the cell walls of cotton fibers, and used the data to quantitatively describe surface roughness changes following chemical extraction. Thimm *et al.* (2000) examined celery MFs and showed an increase in diameter associated with drying.

No previous AFM studies have addressed pit membrane (PM) structure which has largely been studied with high-resolution electron microscopy (e.g. Côté 1958; Thomas 1975; Sano *et al.* 1999). Several authors (e.g. Wheeler 1982; Sano *et al.* 1999) have shown that the surface structure of some angiosperm and gymnosperm PMs changes with age, becoming progressively incrustated with non-microfibrillar materials. The microscopy technique they used required that a thin metal coating, 5–20 nm thick, be deposited on the surface prior to imaging. This coating precluded imaging of features on the surface of the sample that had vertical dimensions of only a few nanometers. In addition the sample had to be placed in a vacuum, and sometimes heated or dried, which could have altered the structure of nanofeatures.

Earlier physiological studies suggested that nanometer-sized particles in the xylem sap might pass through PMs (Choat *et al.* 2003) although appropriately-sized pores were not detected on the surface of the PM by electron microscopy. It has also been suggested that transpiration can be regulated by the ionic composition of xylem sap (Zwieniecki *et al.* 2004), presumably a consequence of PM carbohydrates that alter their conforma-

tion, and therefore the permeability of the PM, in response to changes in ion concentrations. So it became interesting to use the AFM to determine if dried PMs that had not been coated with metal prior to observation might have pores of sufficient diameter to allow nanoparticles to pass, or if the structure of never-dried PMs might reveal a highly permeable arrangement of structural elements. *Sapium sebiferum* is a fast-growing tree species common in the southeastern U. S. A. The structure of its wood is being assessed in our laboratories as it might relate to possible commercial utilization.

#### MATERIALS AND METHODS

Samples were obtained during March 2000–June 2002 from trees approximately 15 m tall in Lafayette parish. For wood that was to be observed dry and without chemical fixation, samples were taken from 1 m long logs that were approximately 18 cm in diameter at 1.3–2.3 m above ground level. The wood was allowed to air-dry for 2+ months in an air-conditioned laboratory room. Tangential sections were taken with a razor blade from either the outermost sapwood or the juvenile wood near the center of the stem. Sections were examined with a  $\times 60$  microscope to determine which areas had exposed pit membranes. These areas were carefully cut away from the surrounding wood, gently pressed onto metal stubs coated with sticky tabs, trimmed further to reduce the overall size of each piece to approximately a 1-mm-sided triangle, and left overnight so that there would be no movement during observation due to drying or mechanical tension release.

Some samples were fixed prior to observation. For fixation in the field, 3 cm<sup>3</sup> pieces of freshly cut wood were immersed into 3.7% formalin in 125 mM sodium phosphate buffer (pH 7) for 18 hours, and then rinsed in water and allowed to air-dry. Alternatively, transverse slabs approximately 2.5 cm thick were cut from a standing tree with a chain saw (Stihl Model #039). The slabs were transported to the laboratory in less than 1 hour where slivers were cut from them with a razor blade and exposed to osmium tetroxide vapors for 1 hour.

Air-dried wood was either sectioned dry or infiltrated with 50/50 ethanol/water. Sectioning was done either with a AO model 860 sliding microtome or with a hand-held razor blade. Sections were placed between weighted glass slides and dried at 50°C overnight.

For imaging a Digital Instruments Dimension 3000 AFM was used. Dried samples were imaged in the tapping mode with LTESP tips (250  $\mu$ m cantilever length). Images were captured at a 512  $\times$  512 resolution. Scan speed was between 2.0 Hz to 0.3 Hz. The RMS voltage when the tip was not engaged on the surface was approximately 1 V. When phase images were captured the amplitude setpoint was lowered from approximately 0.8 V (commonly used for height imaging) to 0.6 V to increase the phase signal. Use of this lowered offset increased the contribution of sample hardness to the phase signal, in contrast to differences in sample viscosity that comprised the majority of the phase signal when the offset was not lowered. A 180 degree phase offset was used to filter-out low phase angle signals.

Three types of data are presented at various points throughout this publication. The most frequent is referred to as the 'height image' which is derived from calculating the

position (in the Z axis) of the tip based on the voltage change needed to return it to its original height after deflection has occurred. This voltage change can be precisely calibrated and serves to determine the height of the feature beneath the tip. A second type of data is the 'phase image' which is derived from the phase angle of the oscillating tip. Phase data is used to determine if the sample contains areas with different physical properties such as hardness. A third type of data is referred to as the 'amplitude image' and is derived directly from the change in the height of the tip, but is not calibrated, so it cannot be used to quantify roughness. Like the 'height image' the 'amplitude image' shows topographic relationships but presents them as a shadowed image from which surface details can be clearly visualized.

In order to locate the actual surface of a dried PM, the AFM tip was inserted into the cavity formed when the plane of fracture formed during sectioning passed over, not through, the surface of the PM. A difficulty with this method was that it made it impossible to observe the junction between the adjoining cell wall and the PM. In addition, there were frequently loosely attached filaments of wall material attached to the pit chamber wall that interfered with the movement of the tip. Nevertheless, by using this method, it was still possible to acquire a large number of scans showing portions of the actual surface of the dried PM.

Intervascular pits were differentiated from vessel/ray parenchyma pits because the latter were small and in relatively small clusters, and the distinctive outline of parenchyma walls could be visualized with the video camera of the AFM. Occasionally, due to the angle of incidence of the fiber optic light, the images provided by the AFM video camera were not always sufficient to enable a precise distinction to be made between pit membranes, and reflective pit chamber walls. This was especially true for unfixed material. To expeditiously locate intact pit membranes for AFM, some unfixed sections were first located (uncoated) with a field emission JEOL 6300FV SEM at 1 kV at magnifications of no more than  $\times 330$ . Using a small SEM spot size and limiting the overall observation time to less than 5 minutes enabled pits to be scanned without causing any noticeable distortion of the vessel element cell walls.

To determine if some PM components could be selectively extracted, a solution composed of 5 ml of glacial acetic acid, 4 ml deionized water, and 1 ml of 30% hydrogen peroxide was prepared. Sections that had previously been imaged while dry were immersed in the solution at 48 °C for 2 hours. Next they were immersed in deionized water at the same temperature for 18 hours, rinsed quickly in two changes of deionized water, blotted dry and placed on a clean glass slide for 12 days at room temperature. The sections did not appear to flex during the extraction procedure and so, after they had been thoroughly dried, they could be placed on the original stubs and their general morphology on AFM video screen could be compared with images taken prior to extraction to thereby locate the same pit membrane that had been imaged prior to extraction.

Non-dried samples were imaged in deionized water or 1 M KCl. Transverse slabs from trees that were approximately 15 cm in diameter at breast height and 2 cm thick were cut with a chain saw and immediately placed in tap water. The slabs were next cut into pieces that fit the sliding microtome chuck and either sectioned and observed immediately, or stored in tap water with 1 mM sodium azide at 4 °C. Sections approxi-

mately 150  $\mu\text{m}$  thick were examined with a light microscope to locate a vessel that had exposed pits and then were bound to a steel plate with rubber bands and imaged while submerged in a plastic Petri plate. An oxide sharpened silicon nitride tip with a V-shaped cantilever 120  $\mu\text{m}$  long and 15  $\mu\text{m}$  wide (each leg) was used.

## RESULTS

### *Low-magnification perspectives of the dried pit membrane*

The structure of the PM varied significantly, even when adjacent PMs were observed, and so it was necessary to clearly identify the actual surface of the PM in order to distinguish it from the surface of internal layers that had been exposed by fracturing. To do this, we adopted a method used by at least one previous investigator (R. Dute, personal communication) which involved observation of PMs in instances where a fracture had passed only through the pit chamber wall, missing the PM completely, and unambiguously exposing the actual dried surface of the PM (Fig. 1 & 2). The phrase 'actual surface' is used here to indicate the surface of the PM that is exposed '*in vivo*', in contrast to a surface exposed as a consequence of fracturing or sectioning. The dried surface of the PM was covered with a reticulate layer of MFs (Fig. 2). Frequently, an abrupt structural and topographical transition occurred between the PM and surrounding wall material (Fig. 1 & 2). In other instances, the plane of fracture passed through the PM making it appear as a two-layered structure (Fig. 3). In Figure 3, both layers are heavily coated (with a material to be discussed in the succeeding results) making it impossible to detect MFs at this magnification. Nevertheless, upon closer inspection at higher magnification it was always possible to determine if a reticulate layer of MFs was present and thereby unambiguously identify the actual dried PM surface.

### *PM structure in dried sapwood from the outer growth ring*

When the plane of fracture passed over, and not through, the PM it was evident that the dried surface was a complex structure composed of three components:

- 1) Microfibrils (MFs) arranged in a reticulate pattern. MFs ranged in width from 25–50 nm and in height from 1.5–4.5 nm (Fig. 4 & 5). Although MF are approximately round in cross section, the width range reported here is probably inflated due to tip broadening (Thimm *et al.* 2000). Given the extreme accuracy of the AFM for vertical measurements, the height range is less problematic although there is bound to be a certain element of inaccuracy because the MFs were on a non-flat surface making it likely the value is an underestimate.

- 2) Irregularly shaped, somewhat globular materials 25–250 nm in width and 11 nm in height that were interspersed among the MFs (Fig. 4–7). The presence and number of globules on the surface was variable, occasionally occurring both in fixed and unfixed samples.

- 3) A thin coating that was composed of at least two components (Fig. 4–16).

The coating was present in all types of dry samples that were examined including unfixed wood (Fig. 8–11, 15, 16), osmium tetroxide-fixed wood (Fig. 4–7), and formaldehyde-fixed wood (data not shown). The extent of coating varied, even when

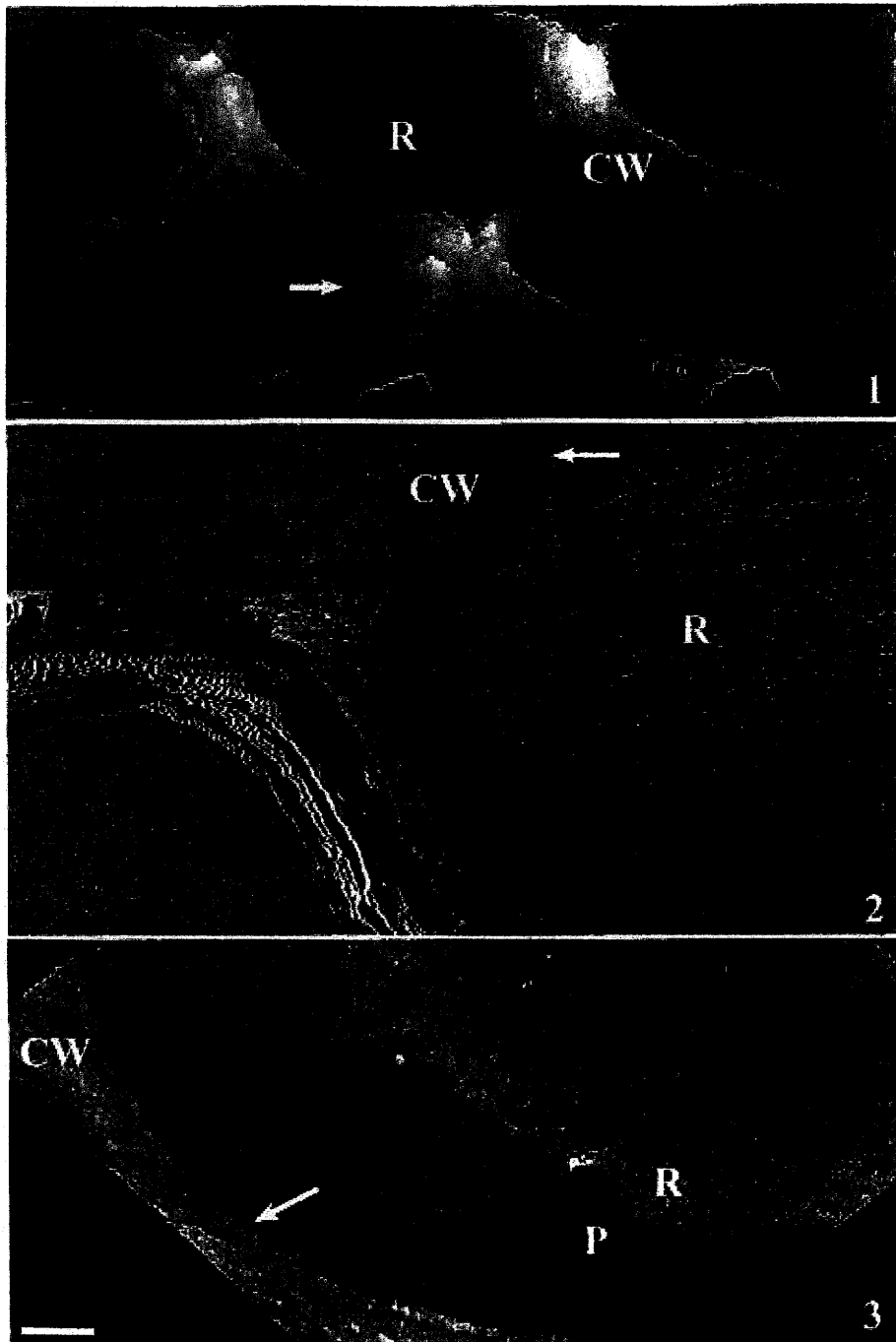
adjacent PMs were compared. When sparse, the coating was predominantly interstitial and located almost exclusively in crevices between MFs and the globular materials (Fig. 4–7). In phase images (Fig. 5, 7, 9, 11, 13–15) it was evident that the coating was phase dark, as opposed to the phase bright MFs and globules, indicating that the coating was either relatively soft or viscous. This phase difference was routinely seen in both the trace and retrace images, as well as in scans taken perpendicularly to the original scan axis, thus assuring that the phase differences were not merely topographical effects (data not shown). The thickness (i.e. vertical dimension) of the coating varied from 1.5 nm to as much as 7 nm, although the 2–5 nm range predominated. Where the coating was moderate it appeared as a network (Fig. 6, 7, 10, 11). This network was sometimes dispersed irregularly across the surface of the PM with some areas having no coating and adjacent areas being coated (Fig. 6 & 7). In cases where the coating was nearly continuous it formed a plaque that had numerous small holes in it (Fig. 8 & 9). Each hole represented an area where an MF or globular material was partially exposed, and was therefore phase bright. Comparison with the corresponding height image dramatically showed the direct relationship between the coating and phase dark areas. In extreme cases, the surface of dried mature PMs located in the outermost ring was completely coated so that MFs were covered (Fig. 12 & 13).

Where the coating was extensive, a phase gray component of the coating (i.e. a component that was intermediate in brightness between the surrounding phase bright and phase dark materials) was frequently observed (Fig. 9, 11, 13, 14). The phase gray material occurred *on top of the coating* as low ridges that were less than 0.5 nm in thickness (Fig. 12). In some cases no phase bright material occurred and the surface of a PM was entirely covered with phase dark and phase gray materials (Fig. 13). The phase gray material was surrounded by phase dark material and was thereby segregated away from the phase bright regions (Fig. 14). Therefore it did not appear to represent a physical intergradation between the phase dark and phase bright material. To sum,

*(Text continued on page 408)*

**Figure legends:** All images are of vessel element PMs, or the adjacent cell wall. The first word in each legend is either 'Height', 'Phase', or 'Amplitude'. This indicates the acquisition mode of each image. Figures 1, 3–16 and 19–23 show air-dried and dry-sectioned material. Figures 1, 2, 17, 18 and 24–29 show air-dried material sectioned in 50% ethanol. Figures 30–36 show non-dried outer growth ring, earlywood PMs sectioned and observed in deionized water. In all cases, *there is only one scale bar per plate* and it is located in the lower left-hand corner of the plate.

**Fig. 1.** Height. Fracture through pit chamber wall (CW) and over actual surface of pit membrane (R). Arrow indicates abrupt transition between PM and pit chamber wall. Scale bar = 2  $\mu\text{m}$ . — **Fig. 2.** Phase. Sectioning removed upper portion of pit chamber wall and revealed actual surface of dried PM composed mostly of reticulately arranged, phase bright microfibrils (R). Arrow indicates region of abrupt transition between PM and pit chamber wall. CW = pit chamber wall. Juvenile wood harvested August 2000. Scale bar = 0.80  $\mu\text{m}$ . — **Fig. 3.** Height. PM with both actual surface and layer beneath it exposed. MFs are heavily coated and so neither layer appears microfibrillar at this magnification (see following for images of MFs with different amounts of coating). R = actual surface; P = surface of internal layer exposed during sectioning/fracturing. Arrow indicates junction between PM and pit chamber wall (CW). Early wood or middle wood, outer growth ring, harvested Aug. 2000. Scale bar = 0.75  $\mu\text{m}$ .



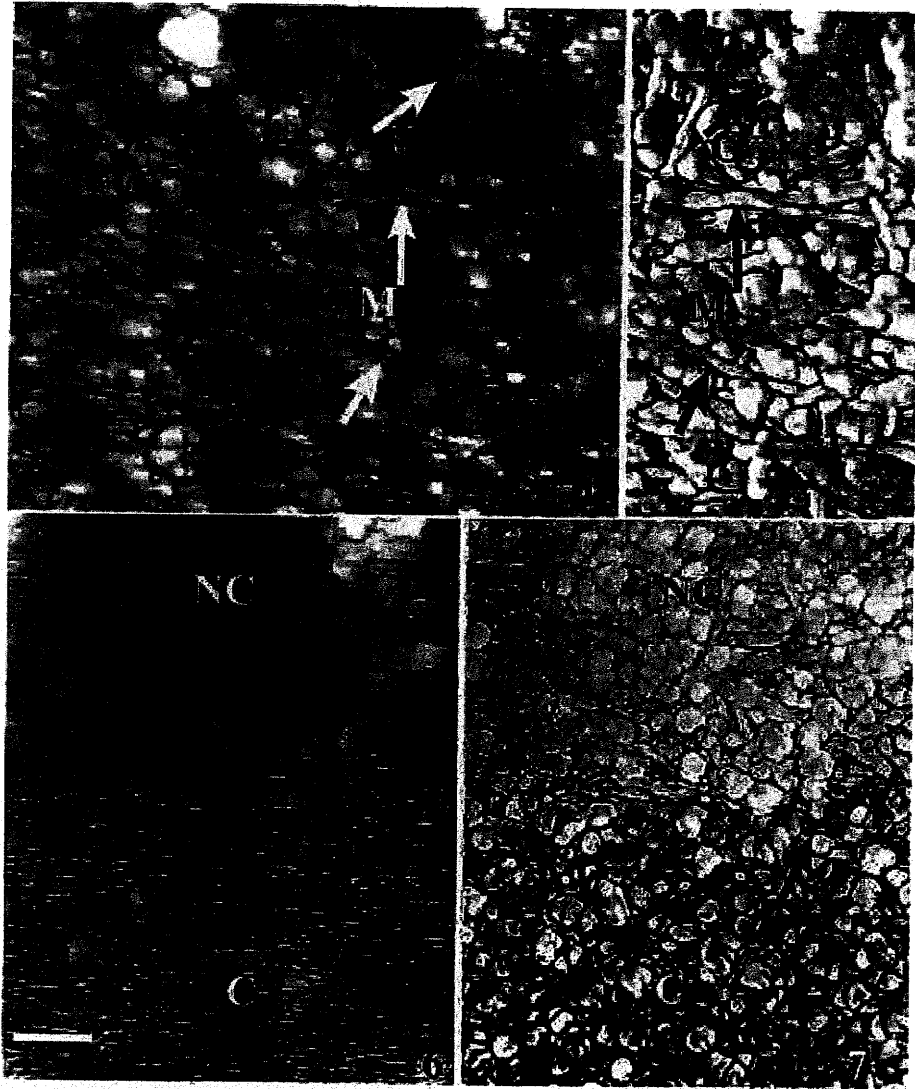


Fig. 4. Height. PM actual surface composed mostly of microfibrils (M) and globular materials (G). Small amounts of interstitial coating material present in crevices (unlabeled arrow). Outer growth ring harvested March 2000, osmium vapor-fixed. Scale bar = 100 nm. — Fig. 5. Phase. Portion of surface seen in Fig. 4. Microfibrils (M) and globular materials (G) are phase bright. Reticulate interstitial coating is phase dark (unlabeled arrow). Arrows point to same positions indicated in Fig. 4. Scale bar = 100 nm. — Fig. 6. Height. PM actual surface is composed of MFs and globular materials. In lower half of image the coating (C) is reticulate and more extensive than in Fig. 4 & 5 although the anatomical location within the stem, time of harvest and method of fixation were identical. Other areas near the top of this figure have little or no coating (NC). Arrows point to identical positions with coating in Fig. 6 & 7. Outer growth ring harvested March 2000, osmium vapor-fixed. Scale bar = 258 nm. — Fig. 7. Phase. Portion of surface seen in Fig. 6. The bottom half of this figure is more phase dark due to the presence of extensive coating (C), while the areas near the top of this figure are almost entirely phase bright due to the absence of coating (NC). Scale bar = 258 nm.

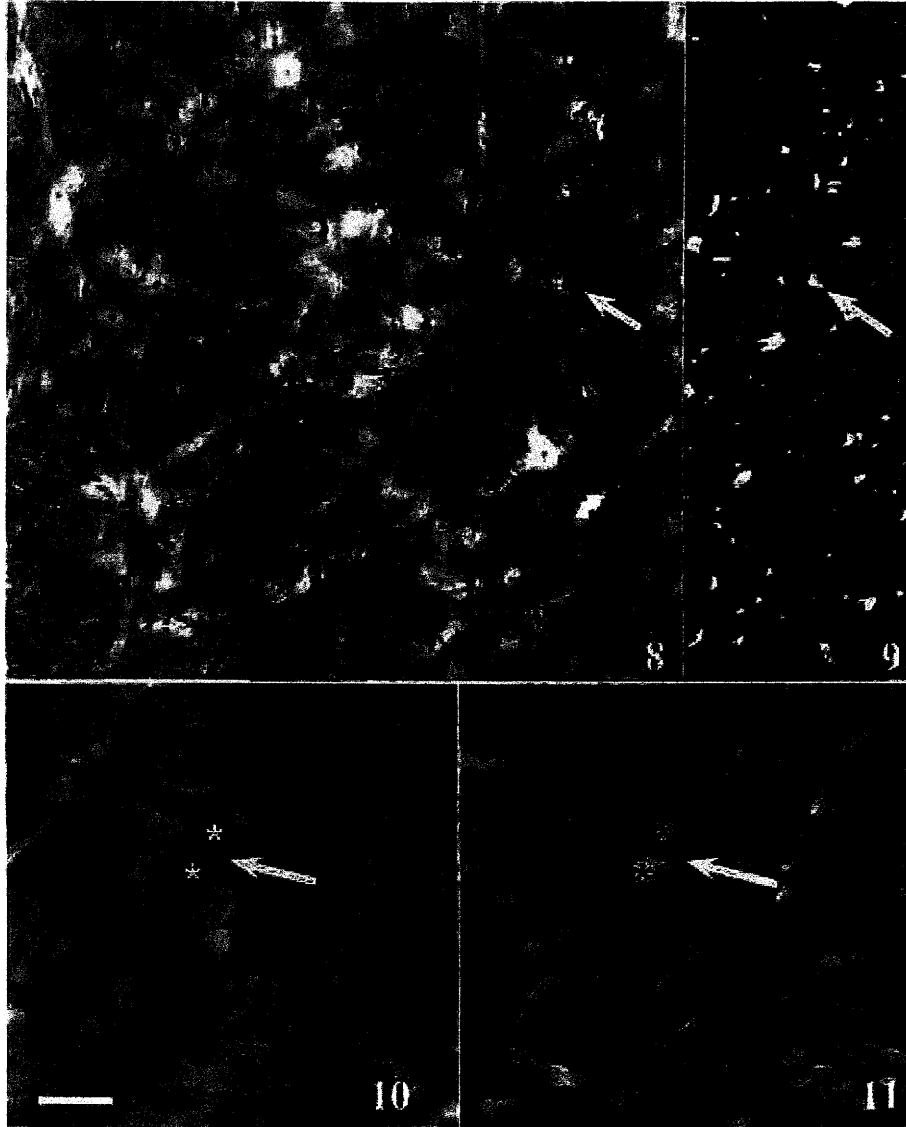


Fig. 8. Height. Coating covers much of the actual surface. Arrow indicates a slight depression (dark area) on the surface where the coating is not present. Middle to early wood, outer growth ring, harvested August 2000. Scale bar = 223 nm. — Fig. 9. Phase. Portion of the PM seen in Fig. 8. Arrow indicates same region indicated in Fig. 8 but here the MF is phase bright indicating that it has a different physical property (s?) from the phase dark coating that surrounds it. Scale bar = 223 nm. — Fig. 10. Height. Coating covers much of the actual surface. Features are similar to those seen in Fig. 8 & 9 but at a higher magnification. Arrow indicates a coated, bridge-like raised area (bright) between two depressions (asterisks). Height of bridge-like area is approximately 5 nm. Middle to early wood, outer growth ring, harvested August 2000. Scale bar = 82 nm. — Fig. 11. Phase. Asterisks mark phase bright areas which correspond to the depressions that are indicated in Fig. 10. There is a close correspondence between the phase bright areas in this figure and the dark depressions in Fig. 10. Scale bar = 82 nm.

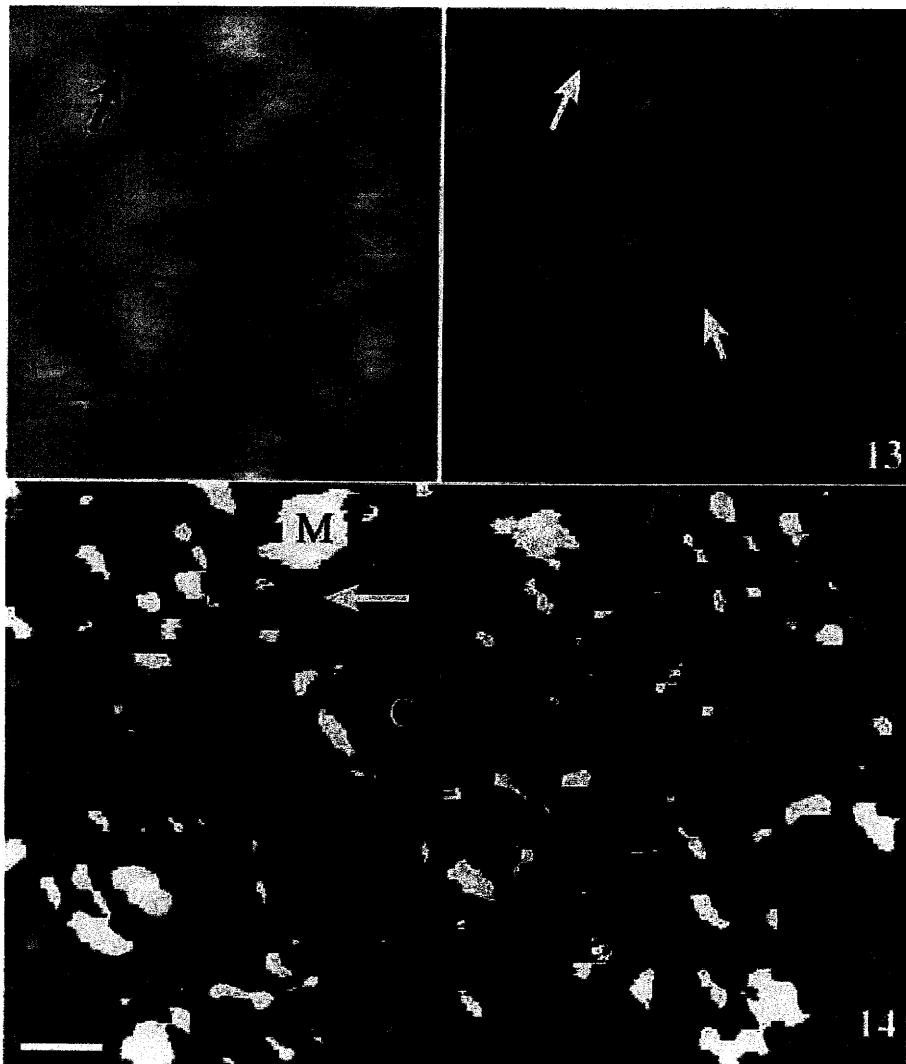


Fig. 12. Height. Coating covers the actual surface (i.e. no MFs or globular materials are uncoated). Contrast is low because of limited surface topography. Arrows indicate extensive system of low (i.e. 0.2–0.5 nm) ridges on top of coating. Youngest mature vessel elements, outer growth ring, harvested August 2000. Scale bar = 78 nm. — Fig. 13. Phase image of area seen in Fig. 12. Arrows indicate same points as in Fig. 12. Low intensity phase brightness here corresponds to the system of low ridges indicated in Fig. 12 and is not from MFs or globular materials located beneath the coating. The phase intensity is reduced in comparison to the brightest areas in Fig. 14 and is here described as being phase gray. Scale bar = 78 nm. — Fig. 14. Phase. PM surface showing three types of phase data in one area: phase dark (C) which corresponds to a coating; phase gray (arrow) which is a very thin layer on top of the phase dark coating and phase bright (M) which is due to MFs or globular materials that are located below the coating. Note that the phase gray material is almost always positioned so that it does not directly border the phase bright material. Instead, there is phase dark material located between the phase bright and phase gray areas. Middle of outer growth ring harvested August 2000. Scale bar = 79 nm.

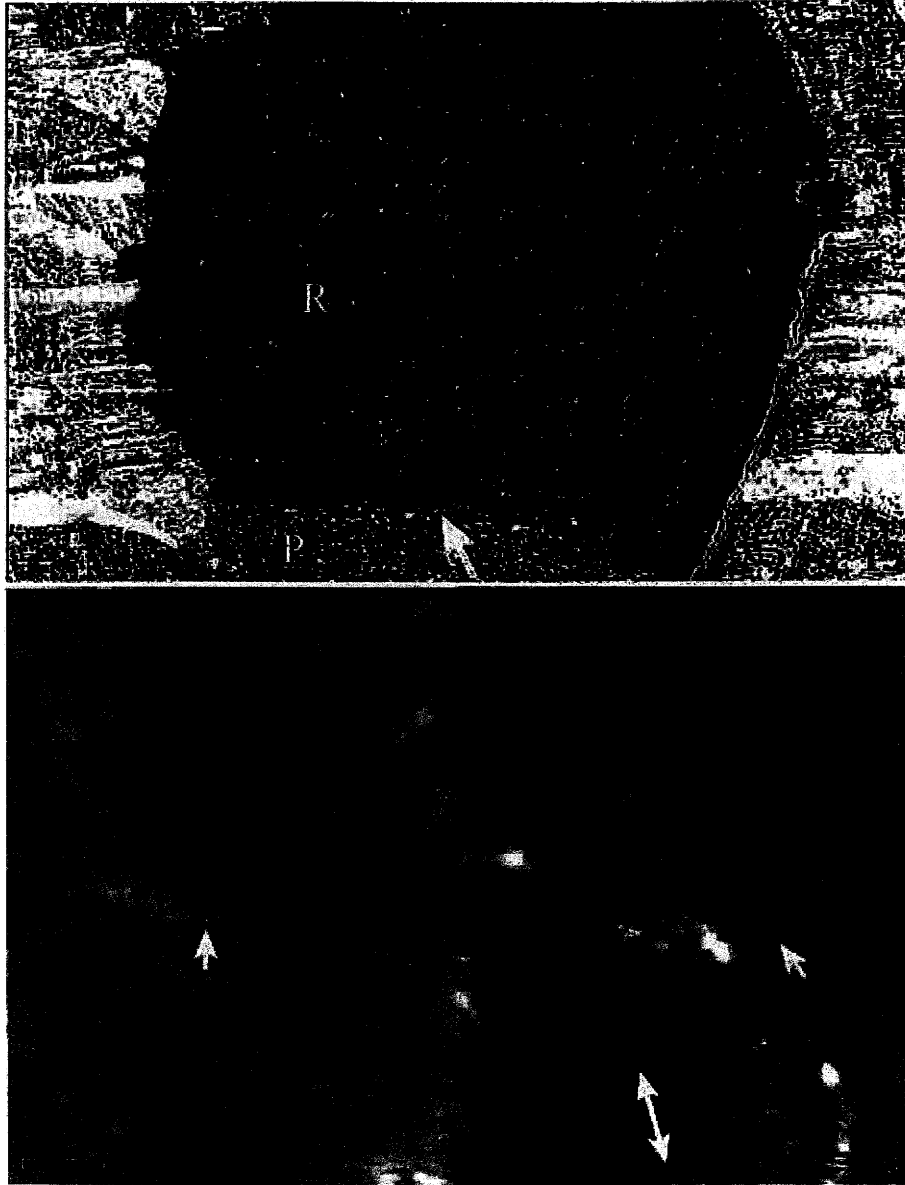


Fig. 15. Phase. PM surface (R) and fractured layer (P) showing relatively phase dark surface. Arrow indicates area shown in Fig. 16. Middle of outer growth ring, harvested August 2000. Scale bar = 670 nm. — Fig. 16. Height. Area indicated with arrow in Fig. 15. Reticulate organization (R) of heavily coated MFs is evident in the surface layer but the coating partially obscures the parallel organization (P) within the fractured layer although some evidence of it can be seen (double arrow indicates apparent direction of underlying MFs). Unlabeled arrows indicate edge of reticulate layer. Thickness of reticulate layer along this edge is approximately 18 nm. Scale bar = 161 nm.

the phase gray material had a distinctive web-like, rather than fibrillar or globular morphology, and a very low side-wall height.

When wood was simply air-dried (i.e. w/o fixation) and sectioned dry, there was a higher incidence of fractures in which the reticulate surface layer of the PM was either fully or partially removed (Fig. 3, 15, 16) to reveal an underlying layer with different surface features. In many cases the phase characteristics of these two surfaces were dissimilar with one being more extensively coated and therefore the darkest. Frequently, the large amounts of coating material that surrounded the MFs of the underlying layer obscured them, making a precise analysis of the microfibrillar array problematic (Fig. 16). However, as a general rule, the underlying surface had MFs that were aligned parallel with each other instead of being reticulate. Where some of the reticulate layer remained, and so formed a ledge that rested on top of the underlying layer, the thickness of the reticulate layer was measured and was found to be in the range of 13–23 nm.

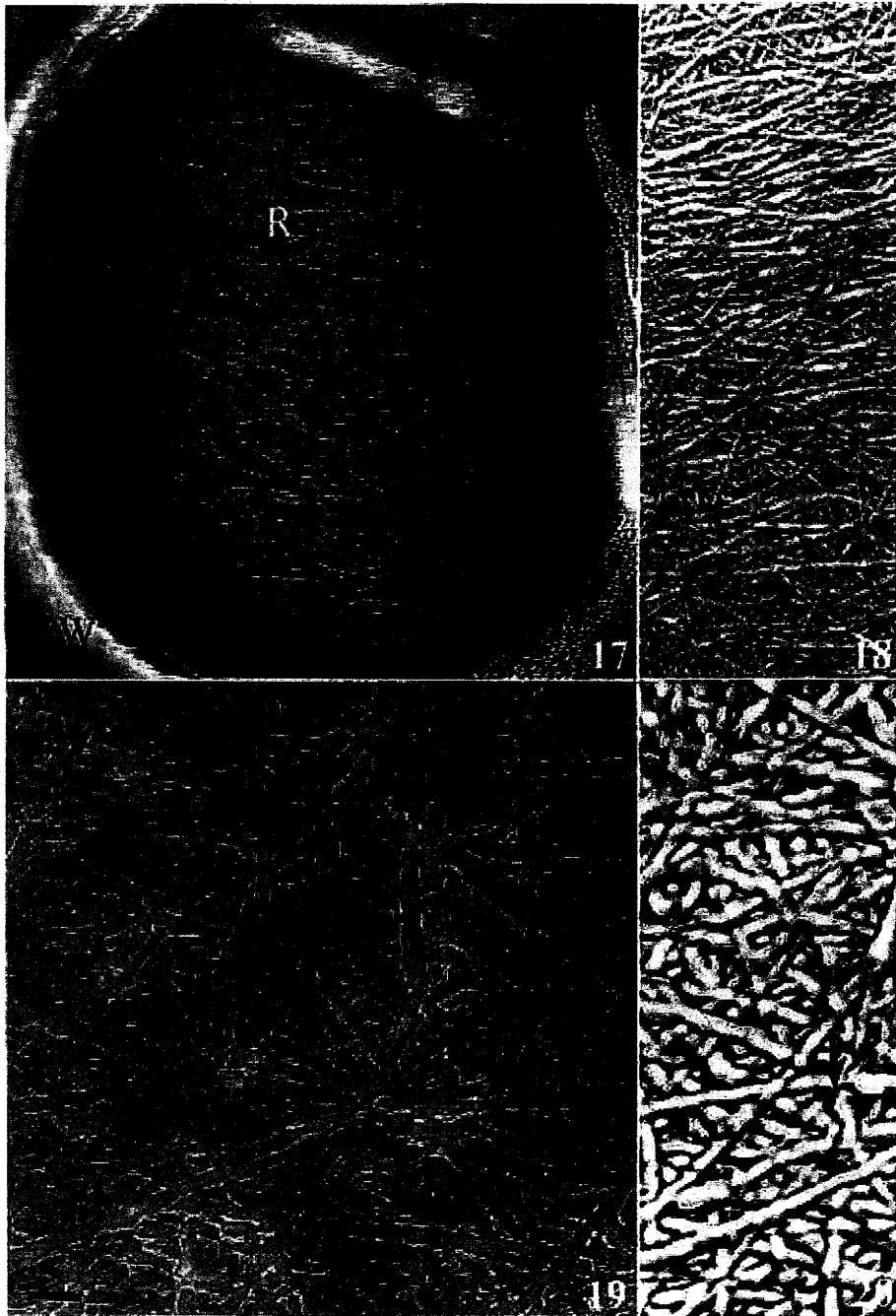
PMs from outermost mature vessel elements that were harvested in November when the tree was physiologically quiescent (i.e. only a few green leaves remained on the branches) were completely covered with non-microfibrillar, granular material (data not shown) and were generally phase dark.

#### *PM structure in dried juvenile wood*

PMs from the second growth ring from the pith of 8–15 year old stems harvested either in August or March were studied. Although there was a low probability of enzymatic activity in the sample, juvenile wood was chemically fixed in some cases for comparative purposes. No consistent differences were noted between fixed and unfixed materials (i.e. both the presence of globular materials and the extent of coating was highly variable), as was the case for sapwood.

The actual surface of dried juvenile wood was predominantly composed of reticulately arranged MFs but was only coated with interstitial material that did not form extensive plaques (Fig. 17–20, 22) as was sometimes observed in PMs from the outermost growth ring. The height of the interstitial coating material was similar to that found in the first growth ring. Globular materials were occasionally observed on the actual surface (data not shown) but their presence did not correspond to whether the wood had been fixed or not. The surface layer occasionally merged directly into the surrounding wall and thus became continuous with the same layer of adjacent PMs (data not shown).

Fig. 17. Height. The plane of fracture/section has passed through the pit chamber wall (CW) rather than through the PM, and so the PM surface is visible. The organization of the MFs is reticulate (R). At this magnification, the presence of a coating is not evident. Second growth ring from center of tree (juvenile wood approximately 15 years old) harvested August 2000. Scale bar = 790 nm. — Fig. 18. Phase. Juvenile wood vessel element PM surface similar, and at higher magnification, to that seen in Fig. 17. The surface is highly reticulate. A few parallel MFs and globular materials are present. Second growth ring (juvenile wood) harvested August 2000. Scale bar = 342 nm. — Fig. 19. Height. The coating is extensive (arrows), bordering all of the reticulate MFs, but not covering them. Juvenile 8-year-old wood harvested March 2000, osmium-fixed. Scale bar = 112 nm. — Fig. 20. Phase. Portion of area shown in Fig. 19. Arrows indicate the same points as in Fig. 19.



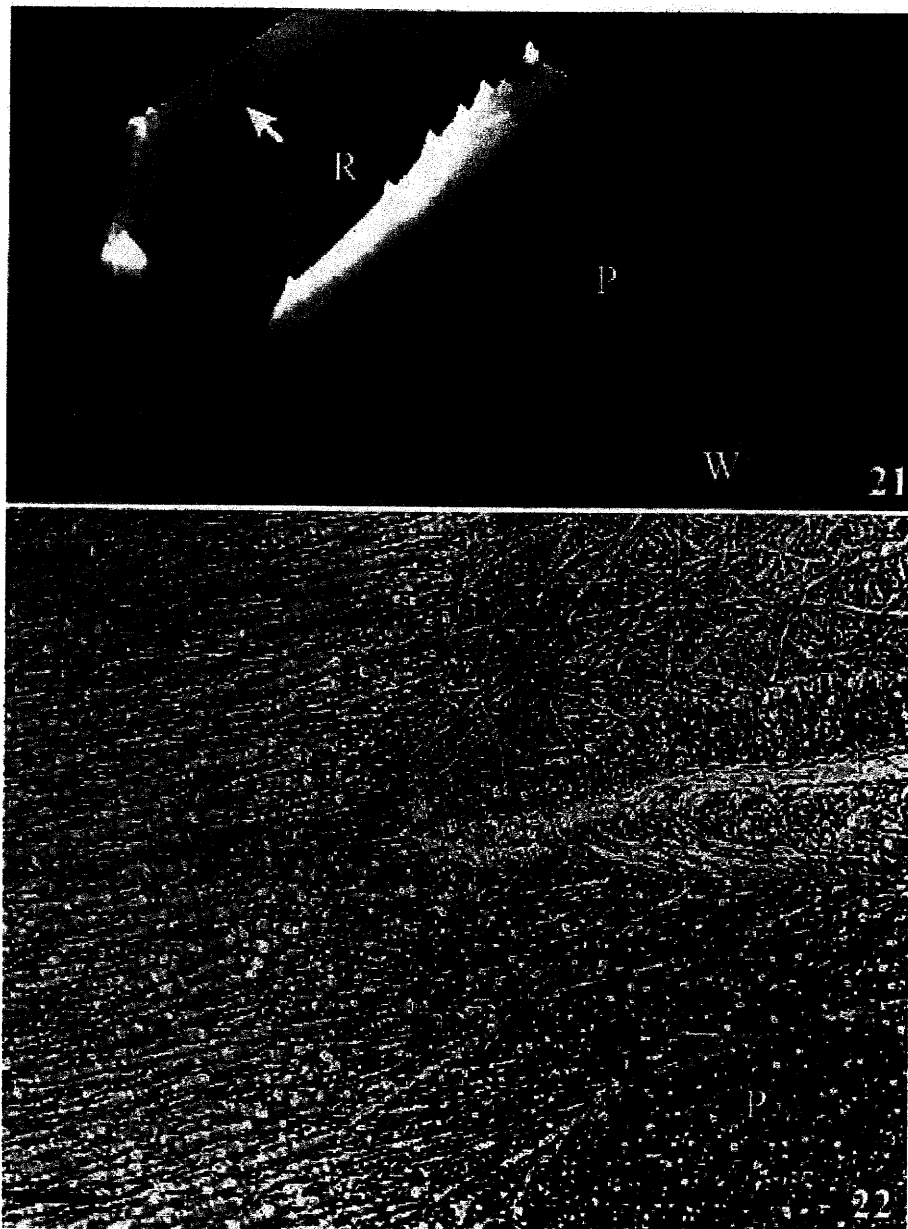


**Fig. 21. Height.** Surface layer (R) is partially detached from underlying layer (P) and curled upward. Border of surface layer is continuous (arrow) with adjacent cell wall, and in some cases this connection extends to adjacent PM as well (not shown here). The underlying layer was always observed to be continuous with the adjacent cell wall (W). Juvenile wood harvested March 2000, osmium-fixed. Scale bar = 1.23  $\mu\text{m}$ . — **Fig. 22. Phase.** PM seen in Fig. 21 at higher magnification showing portion of curled surface layer (R) and underlying layer (P). Adjacent cell wall (W). Increased phase darkness of underlying layer is correlated with reduced visibility of MFs. Scale bar = 284 nm.

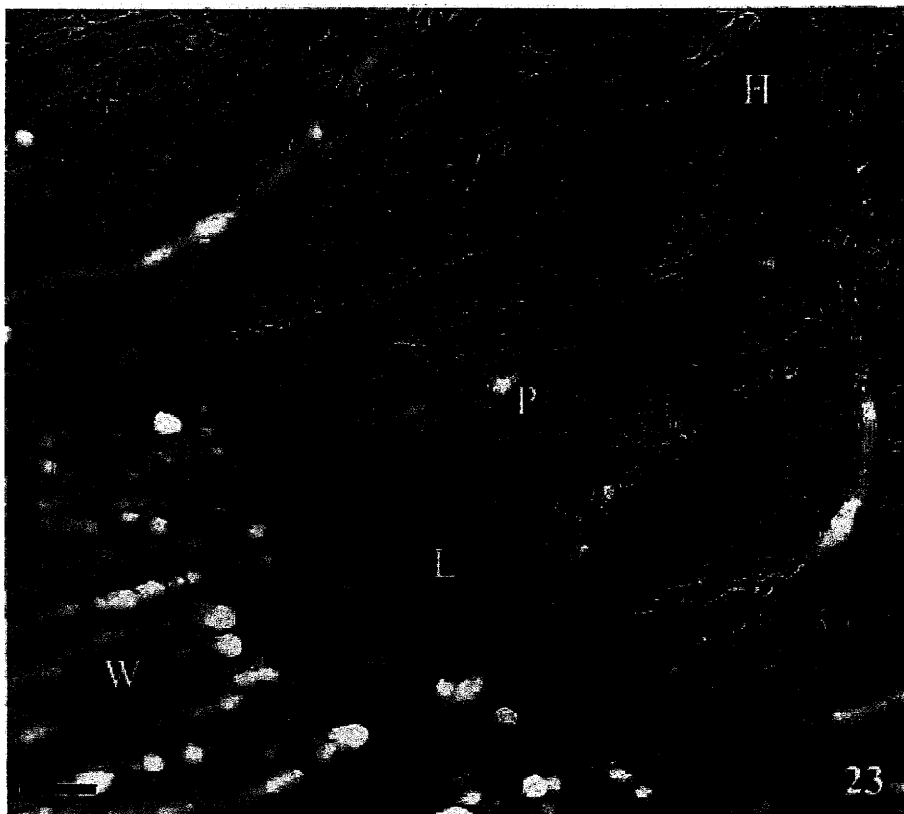


Fig. 23. Height. PM adjacent to that seen in Fig. 21 showing underlying layer (P) with a few MFs running parallel to those in the adjacent wall (W). The amount of coating material increases centripetally so that in the upper right-hand corner the coating is extensive and plaque-like (H) while at the junction of the P layer with the cell wall the amount of coating is much reduced (L). Harvested March 2000, osmium-fixed. Scale bar = 151 nm.

Frequently the PM was fractured or the reticulate layer curled back on itself (Fig. 21 & 22) so that a distinctly different underlying surface became visible. The thickness of the reticulate layer could then be measured and was found to vary within the range of 25–50 nm. The thickness of the underlying layer was not determined because no specimens were found where an edge fracture of this layer was visible. Assuming that the reticulate layer represents half the thickness of the entire PM, then the thickness of the total PM would be in the 50–100 nm range. The margins of the underlying layer always merged directly into the surrounding cell wall (Fig. 21–25). The underlying surface had few visible MFs, possibly because coating was abundant (Fig. 22). However, in some cases, it was evident that numerous MFs were present and were arranged parallel to each other so that they were in line with the MFs in the surrounding wall (Fig. 23). Thus the parallel MFs in the underlying layer were not radially disposed around the center of the PM (as is the case for margo MFs), but rather were oriented in one direction across the PM.

*Chemical treatment of sapwood vessel element PM*

In order to better understand the composition of the PM it was desirable to chemically remove components of specific PMs and observe them before and after treatment. We first imaged air-dried vessel elements to locate morphologically distinct PMs, then dismantled the wood, treated it with acidic peroxide solution, rinsed it in water, then air-dried and remounted it.

Prior to chemical treatment (Fig. 24, 26, 28) PMs showed a variety of structures on the actual surface including MFs (Fig. 24, 28), coating (Fig. 26, 28), and globular materials (Fig. 28). After extraction the PM surface had become extensively altered (compare Fig. 24 with 25). Some of the coating on the dried PM surface still remained after peroxide treatment (compare Fig. 26 to 27), suggesting that the majority of the dried layer had not been removed. In general, the MFs of the reticulate surface had

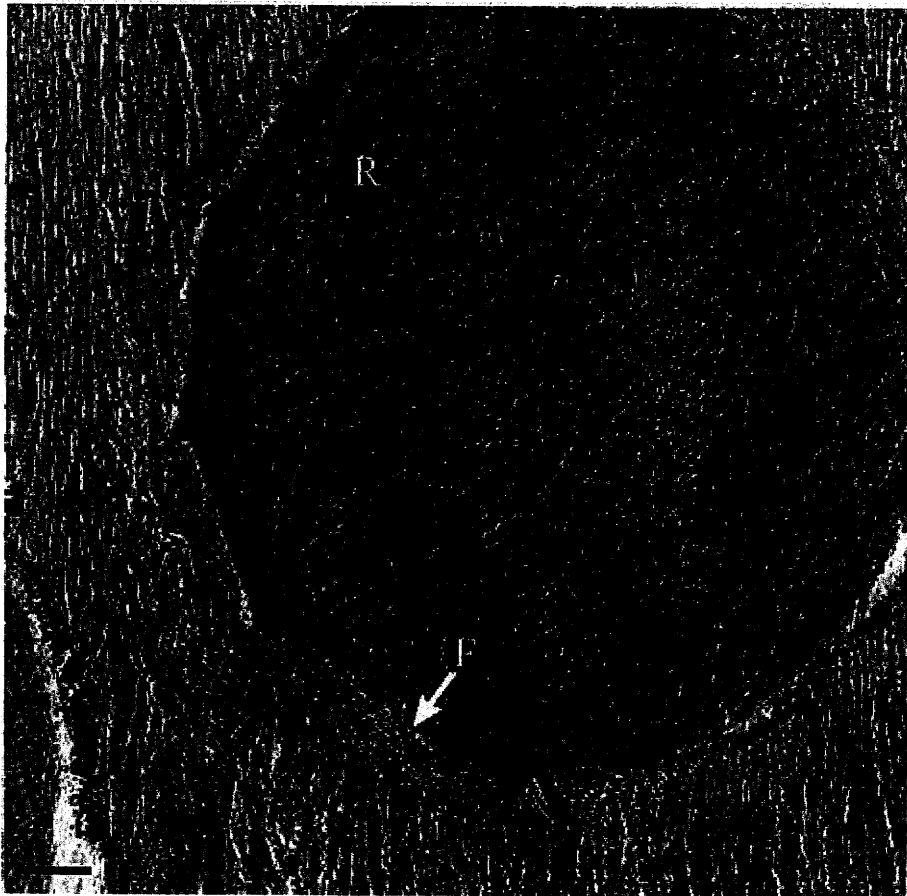


Fig. 24. Height. PM prior to chemical treatment. R = surface with reticulate MFs; F = fractured edge where the underlying layer with parallel MFs is exposed – this is the edge used to measure the height of the R layer. Scale bar = 657 nm.

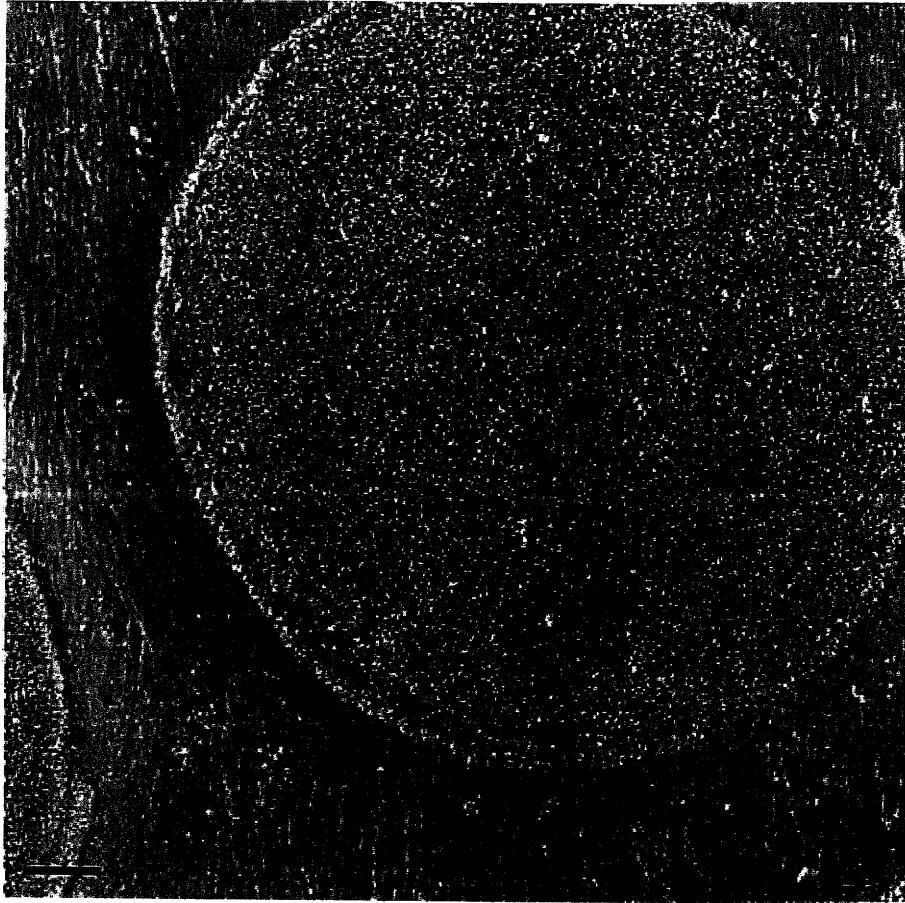


Fig. 25. Height. PM after chemical treatment. R = surface with reticulate MFs (prior to treatment); F = fractured edge where the underlying layer with parallel MFs is exposed – this is the edge used to measure the height of the R layer. Scale bar = 657 nm.

either been removed or altered (compare Fig. 24 with 25, and 28 with 29). The reticulate surface became much more globular in appearance (compare Fig. 24 with 25, and 26 with 27). In contrast to the loss/alteration of the reticulate MFs on the surface, the MFs of the underlying layer appeared to have been retained and exposed (compare Fig. 28 with 29). Surprisingly, at sites where the PM had been fractured, there was no evidence that the thickness of the fractured layer had been decreased by the chemical treatment (measurement data not shown but taken from areas indicated in Fig. 24–27 and others).

#### *Native PM structure in the outer growth ring*

Non-dried PMs exhibited either of two distinct morphologies: microfibrillar (Fig. 30) and non-microfibrillar (Fig. 31). Within groups of PMs, some would show an entirely

non-microfibrillar surface while the adjacent PMs showed a microfibrillar surface (data not shown) indicating that a tip malfunction was not a consideration. Also, the close proximity of such differently structured PMs to each other made it seem unlikely that developmental events caused the differences. Instead it seemed most likely that these structural differences were due to events that occurred during the process of sectioning/fracturing the wood.

*(Text continued on page 419)*

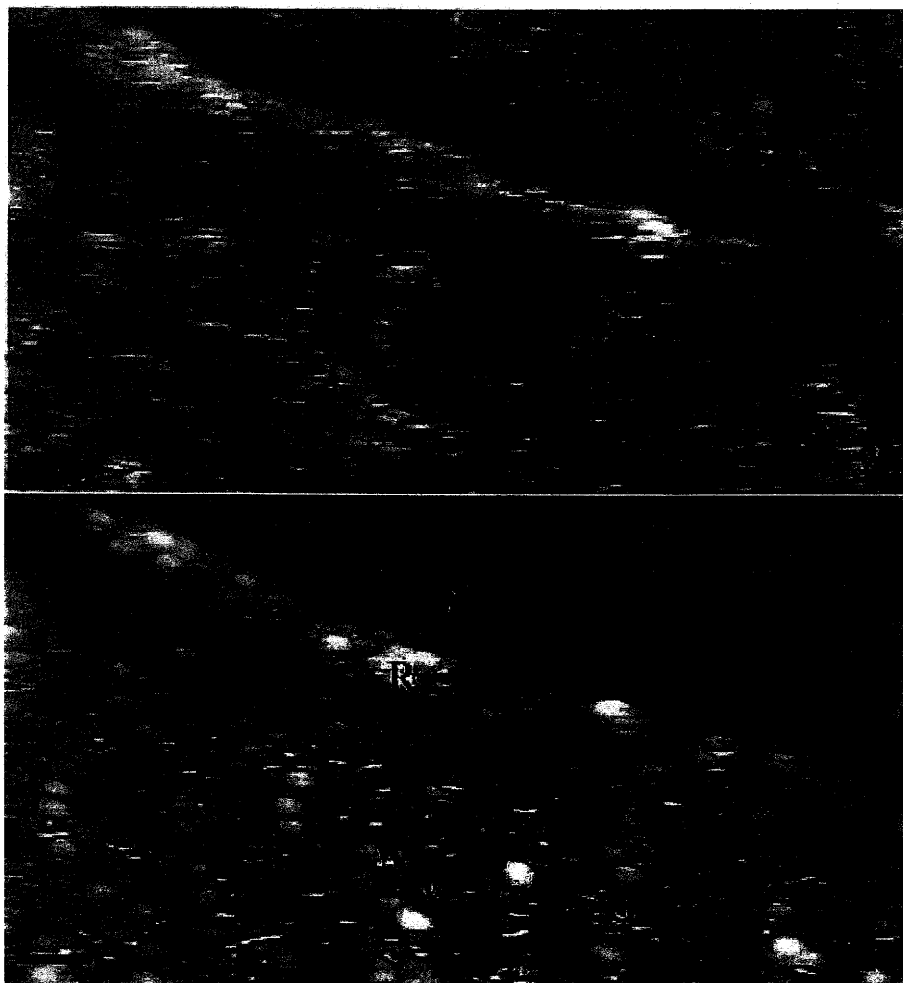


**Fig. 26.** Height. Outer growth ring PM prior to chemical treatment. R = reticulate surface; P = parallel layer exposed by fracturing and located under the reticulate surface; C = plaque-like, extensive coating, present on both P and R surfaces. Dark furrow that runs from top left corner to middle of right edge is the edge of the fractured R layer. Harvested August 2000. Scale bar = 160 nm. — **Fig. 27.** Height. Area seen in Fig. 26, after chemical treatment. The P surface has become slightly wrinkled during chemical treatment. The coating (C) has become much less extensive on both the P and the R surfaces. The R surface consists primarily of globular materials (G).

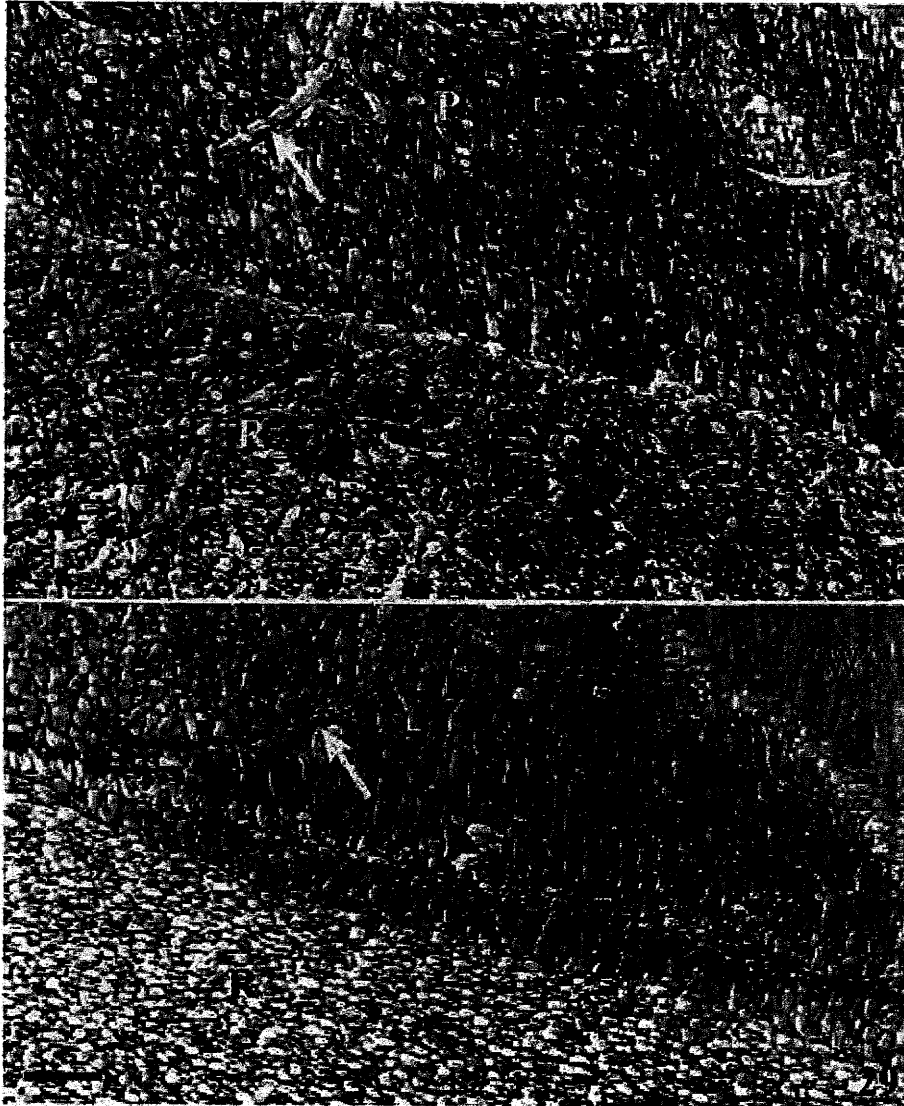
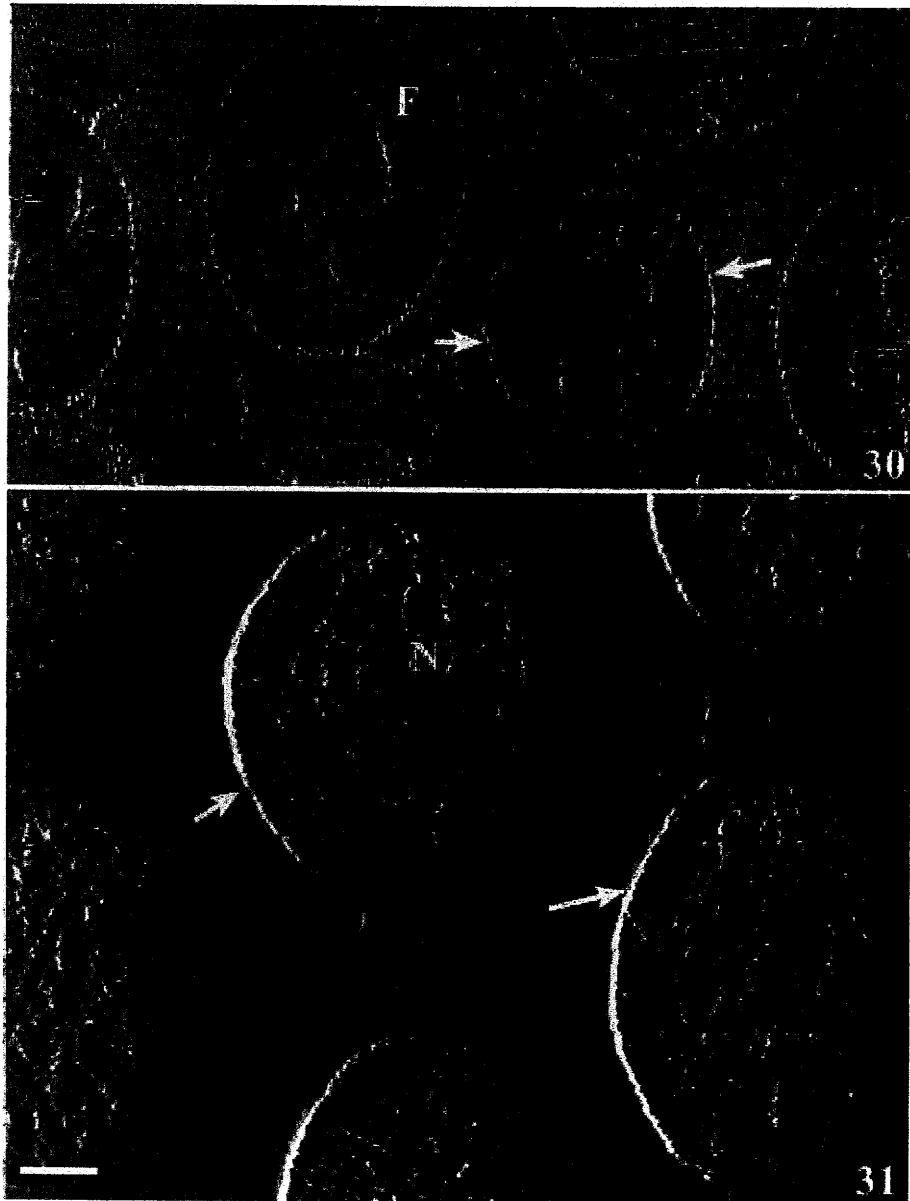


Fig. 28. Phase. Area seen in Fig. 26, but at a lower magnification. The untreated P and R surfaces both display multiple MFs (arrow). Some of the MFs on the P surface are not parallel, presumably due to events occurring during the process of fracturing. The black material corresponds to the coating. Scale bar = 283 nm. — Fig. 29. Phase. Area seen in Fig. 28 after chemical treatment. There are no apparent MFs on the R surface, but the MFs on the P surface are still visible (arrow corresponds to arrow in Fig. 31), and may have become more so. The black coating material that is extensively present in Fig. 31 is much less prevalent.



**Fig. 30.** Height. All of the PMs exhibit a microfibrillar surface (F). While a specific and precise organization of MFs is not obvious, MFs on the sides (arrows) tend to be parallel, while the MFs in the center of the PM seem to be aggregated into a roughly circular, or oval, arrangement. Harvested June 5, 2000. Scale bar = 1.49  $\mu\text{m}$ . — **Fig. 31.** Amplitude. All of the PMs exhibit a non-microfibrillar surface (N) except for some regions at their periphery (arrows) that have parallel MFs. Harvested June 4, 2002. Scale bar = 1.42  $\mu\text{m}$ .

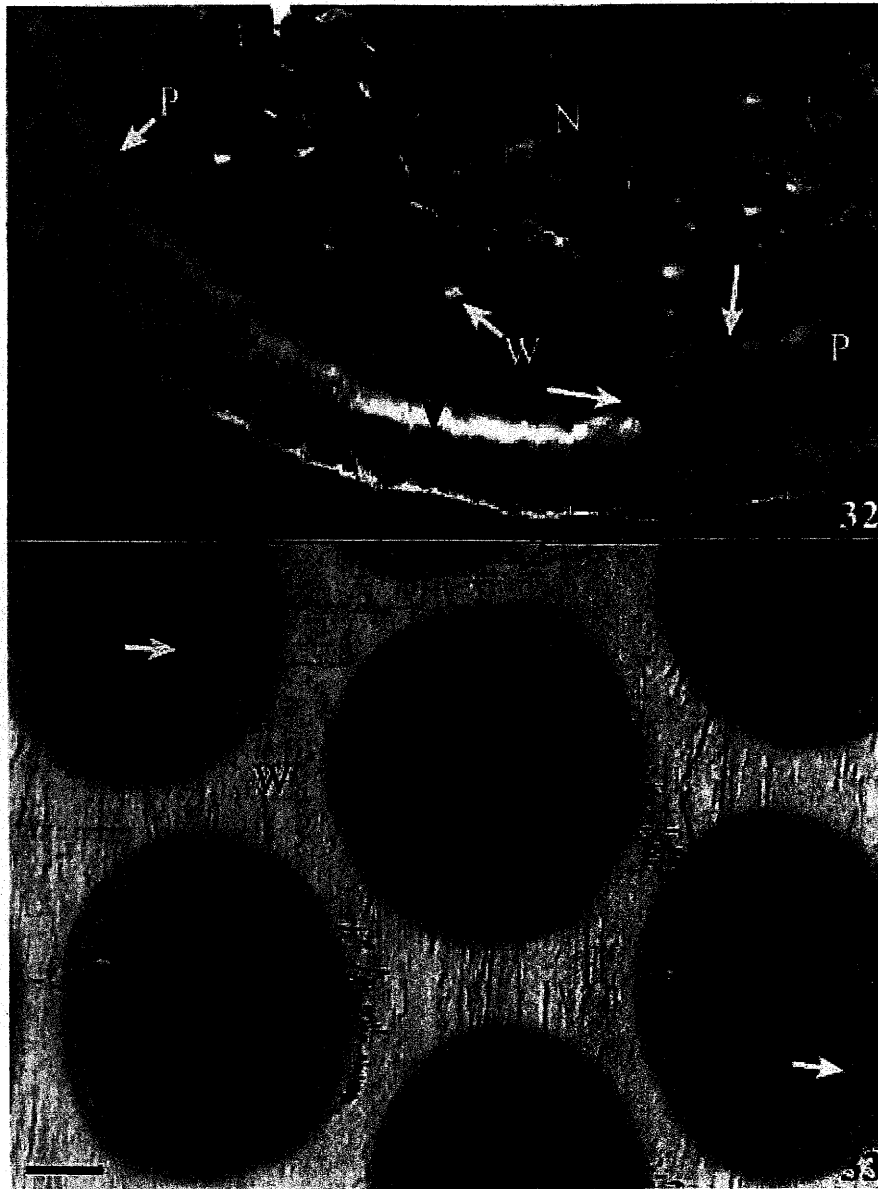


Fig. 32. Amplitude. Only a portion of a non-microfibrillar PM (N) is seen. The PM has apparently been only partially preserved, allowing warts (W) on the pit chamber wall to be seen. The peripheral rim of the PM exhibits an array of parallel MFs (P) that, in some places, extend out to apparently contact (white arrows) the non-microfibrillar portion of the PM. In the center of the rim the parallel MFs overlay each other to form a crossed pattern (black arrow). Harvested May 31, 2002. Scale bar = 478 nm. — Fig. 33. Phase. PMs in Fig. 31. Wall surrounding the PMs is phase bright (W) and the PMs are phase dark. The non-microfibrillar surface of the PM is plate-like or ridged (arrows). This may be an artifact due to tip deformation of the soft and easily deformable surface. Same magnification as in Fig. 31.

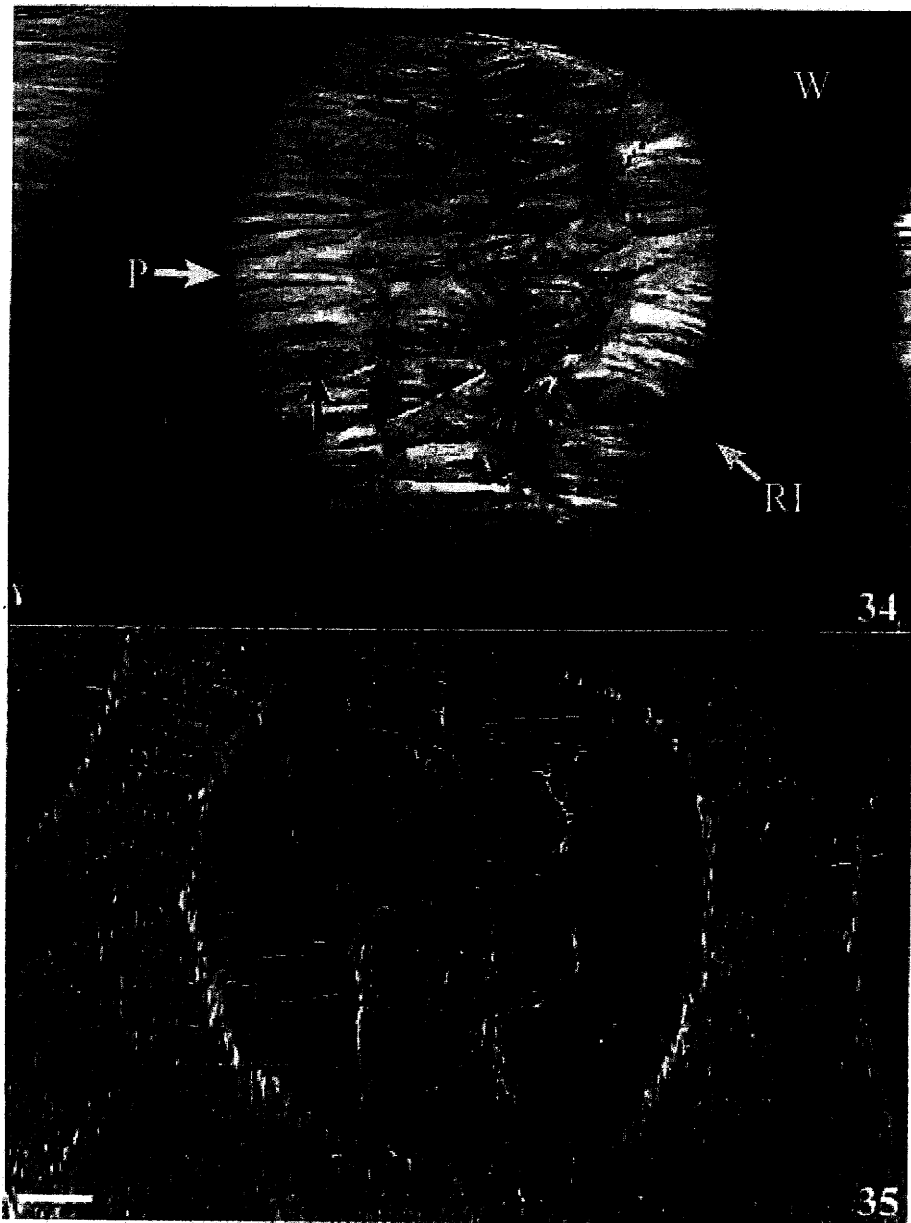


Fig. 34. Phase. Higher magnification of non-dried PM. in Fig. 30. The PM displays an entirely microfibrillar surface and is phase bright, in contrast to the surrounding wall (W) which is phase dark. The parallel microfibrils (P) on either side of the centralized array clearly overlay other MFs (arrows) making it difficult to determine the entire height of the microfibrillar array. A phase gray ring (RI) encircles the microfibrillar PM and may represent a portion of the pit chamber wall. Scale bar = 645 nm. — Fig. 35. Height. Image of Fig. 34 better showing the three-dimensional arrangement of the MFs.

In contrast to dried PMs, in non-dried PMs it was uncommon to observe regions where there was a coating on top of MFs. Instead, some PMs were composed of either distinctly microfibrillar or non-microfibrillar regions (Fig. 31 & 32). Near the periphery of the PM there were instances where microfibrillar and non-microfibrillar structures merged (Fig. 32). Interpretation of the peripheral region was difficult, but the area with crossed MFs in Figure 32 is located where the annulus might be. With the exception of this, there was no visible contact between MFs and the non-microfibrillar portions of the PM.

In some cases, only a portion of the non-microfibrillar surface remained, making it possible to see a portion of the hemispherical pit chamber wall that was apparently beneath it (Fig. 32). The presence of warts on the chamber wall is interpreted as an indication that the vessel element was mature. Here there was frequently more than one micrometer of height difference between the PM surface and the pit chamber wall, suggesting that the PM did not sag down and touch the pit chamber wall but rather was stretched out like a sheet. While the overall thickness of the non-microfibrillar layer was problematic because of the inability of the AFM to detect the presence of overhanging ledges as opposed to sheer vertical walls, topographic features on the surface of the non-microfibrillar layer frequently had vertical dimensions in the 100–300 nm range.

The phase signal of the non-microfibrillar surface differed greatly from that of the surrounding cell wall, which was relatively bright (Fig. 33). The phase signal of the non-microfibrillar surface was generally dark, similar to that of the plaque-like or interstitial coating that was observed on the dried surface. The non-microfibrillar surface frequently exhibited a series of irregular plate-like structures (Fig. 33) due to topography rather than mechanical differences (i.e. the trace and retrace images showed opposite, rather than similar, brightness values, data not shown). When the tip passed over a non-microfibrillar surface it was difficult to produce images of the highest quality (i.e. without streaks in the direction of the scan) suggesting that the surface was easily deformed by the pressure of the tip (Fig. 33).

In instances where a microfibrillar surface was visible (Fig. 30, 34–36) it was possible to obtain better quality images. The phase image brightness of these PMs and the surrounding walls (Fig. 34) were the reverse of non-microfibrillar PMs seen in Figure 33. The surrounding walls were phase-dark while the microfibrillar region was phase bright (just as were the microfibrils in dried PMs). A small ring of intermediate phase bright material occurred around the periphery of the PM, and this could be a slightly raised portion of the pit chamber wall.

MFs in the center of the PM were arranged in a reticulate pattern (Fig. 30, 34, 35) that extended to the PM periphery in some places. The central area of each PM appeared to be a loose knot of MFs with some parallel MFs flanking it on either side (Fig. 30, 34, 35). Some peripheral portions of the PM were composed of MFs that were aligned parallel with each other. The peripheral region of the PM was comprised of branched or overlapping MFs that merged directly with the surrounding cell wall (Fig. 36). Underneath the peripheral MFs were other arrays of parallel MFs that were roughly perpendicular to the upper layer (Fig. 36).

The distance between MFs was highly variable, ranging from a maximum of approximately 300 nm and including numerous instances where more than 100 nm was

to as 'coating' in the present article. Given the techniques used by those authors, it is doubtful that they would have been able to observe the very thin interstitial or plaque-like coatings like those in *Sapium*. In this regard then, it appears likely that the literature from electron microscopy will tend to diverge from that of the AFM. While it could be that *Sapium* is simply different from the earlier-researched species, it is also possible that the ability of AFM to image a very thin coating has revealed that the PM is always associated with some degree of non-microfibrillar surface material. Because the coating is so prevalent throughout the wood of *S. sebiferum* we favor the latter interpretation, but further comparative research with other species is required. In any case, the use of the term 'coating' as observed with the AFM should be understood to indicate at least a quantitatively, and possibly a qualitatively, different surface structure than is indicated by the term 'encrustation' in TEM/SEM studies.

We observed some heartwood PMs with a very heavy layer of non-microfibrillar surface material (i.e. encrusted). The fact that the encrusted surface of heartwood PMs had a phase bright signal suggests that it does not have the same composition as the phase dark coating seen on the surface of PMs from the outer growth ring. Many more heartwood PMs had coated rather than encrusted MFs. This higher frequency suggests that the process of aging affected the mechanical properties of the PM, pre-disposing it to removal of the encrusted layer during sectioning. Wheeler (1981) described instances in which the encrusted layer was removed by fracturing during specimen preparation. The known chemical differences between the encrusted and the microfibrillar layers of the wall in other species (Bauch & Berndt 1973; Parameswaran & Bauch 1975) could provide a structural basis that would increase the probability that fractures could form between these two components of the PM.

At least in dried materials, each PM consists of MFs arranged in layers. The existence of layered pit membranes similar to those reported here for *S. sebiferum* has been reported in other species by Schmid and Machado (1968), Wheeler and Thomas (1981), Wheeler (1981), Dute *et al.* (1990, 1992), and Morrow and Dute (1998). A two-layered pit membrane structure was shown by Dute *et al.* (1990, Fig. 14; 1992, Fig. 14) for the dicotyledon *Daphne mezereum*. There are many possible structural perspectives that can be formulated to integrate these two types of microfibrillar arrays into an overall structure for the PM. The microfibrillar portion of the PM is composed of materials derived from the middle lamella and the cellulosic primary wall layers of two cells (Bonner & Thomas 1972). In a broad sense, this situation resembles that of freeze fracturing where the plasmalemma, which is much thinner than a pit membrane, can be fractured along a plane of weakness that exists along the hydrophobic center of the membrane where lipid tails oppose each other. In wood that has been chemically fixed, or heated, during the drying period the reduced frequency of fractures that reveal two microfibrillar layers points to the importance of chemical factors in the formation of such fractures through the pit membrane. The simplest perspective is that the middle lamella is the most likely breaking point because it consists of a high percentage of non-cellulosic carbohydrates that lack the strong structural properties of polarized cellulosic arrays. If a fracture occurs through the plane of the middle lamella then the parallel microfibrillar array will be the most likely to be exposed. The parallel MFs

will be embedded in a softer, phase dark matrix composed of middle lamella materials, although the plane of fracture is probably not always as precise as that found for cell membranes because of the extensive interlinking between the many types of carbohydrates that comprise the middle lamella and the PM. In support of this idea is our observation that the parallel microfibrillar surface has a large amount of phase dark material associated with it. If the plane of fracture misses the PM, then the actual surface is observed and the predominantly reticulated microfibrillar arrangement will be observed. While this interpretation is attractive because of its simplicity and logic, the situation has, at least, the potential to be more complex because Wheeler and Thomas (1981) observed an amorphous layer under the microfibrillar layer in the outermost growth ring of red oak.

In the dried PM of *S. sebiferum*, the sparsely microfibrillar layer is clearly linked to the surrounding wall by parallel arrays of MFs like those shown in *Goniorrhachis* by Schmid and Machado (1968). They interpreted this latter layer as being primary wall that had been stretched during wall elongation so that the reoriented MFs became parallel. Schmid and Machado also interpreted the reticulate pit membrane layer as being a later-formed portion of the primary wall. Our interpretation of *S. sebiferum* agrees with that in *Goniorrhachis*, an observation that strongly suggests that the basic aspects of pit membrane structure have been conserved within a fairly broad range of angiosperms.

The ability to view specific PMs before and after chemical treatment confirms and extends the usefulness of the AFM as a sensitive analytical tool for the *in situ* analysis of biological structures. The selective action of the acidic peroxide reagent on the reticulate surface layer indicates that the chemistry of this layer differs significantly from that of the innermost region of the PM where the MFs are generally parallel in their organization. The deformation of the MFs in the reticulate layer that is a consequence of acidic peroxide treatment suggests that lignin is a significant component of the PM surface. Likewise, the retention of MFs on the underlying surface may be due to the presence of higher amounts of polyphenolics.

It is necessary to reconcile the images of dried and non-dried PMs shown in this report. The dried images show two layers, both of them microfibrillar, and both with some degree of coating on the MFs. The non-dried images show one microfibrillar and one predominantly non-microfibrillar layer. The relatively thick non-microfibrillar material seen in non-dried PMs could conceivably form the irregular coat that is observed on the dried PM. Possibly, during the process of drying, the non-microfibrillar layer seen in non-dried PMs is displaced onto MFs, thus forming the coating. It is not hard to imagine that an unregulated, somewhat random, process of drying as occurs following harvesting of the wood could unevenly displace a non-microfibrillar substance throughout the network of MFs that make up the inner portions of the PM, resulting in observations of irregularly distributed coatings and globular materials. This idea is supported by the fact that the non-microfibrillar layer in non-dried PMs and the coating materials in dried PMs both have the same properties in phase images (i.e. they are both phase dark).

It is more difficult to reconcile the differences in dried vs non-dried images of MF arrangements. No clear evidence for different layers of MFs is present in the non-dried

PMs. This may be due to the difficulty of forming a fracture through the loosely-packed web of non-dried MFs. It may also be that the relatively complex microfibrillar arrangement within non-dried PMs makes observation of two distinct layers difficult. It is notable that the overall arrangement of non-dried MFs was much less compact than those seen in dried materials both by us and other investigators. This lack of compactness may, to some degree, be a reflection of tearing forces generated during the act of fracturing, but because the same type of loosely interwoven structure was observed in hundreds of cases, there also seems to be significant merit in the idea that the less compact structure is a valid representation of the *in vivo*, hydrated condition where microfibrils are hydrated. While the highly compacted MFs seen in images of dried PMs would tend to refute the assertion that the PM is a conduit for water passage, the images shown here of non-dried PMs, showing relatively open arrays of MFs, are much more in keeping with the type of structure that could be imagined to permit the passage of fluids. In species such as *Sapium sebiferum* the loosely arranged, compressible MFs would permit the passage of water during transpiration, but shrink into a less permeable layer during dry episodes. This functional explanation would fit well with the role of PMs in the reduction of air-seeding as discussed by Cochard *et al.* (1992).

The role of the non-microfibrillar layer is also interesting. Non-microfibrillar, or amorphous, materials have been reported in the torus of presumably functional tracheary elements of several species (e.g. Dute & Rushing 1987; Dute *et al.* 1992; Sano *et al.* 1999). The torus is believed to be a sealing mechanism during periods of water stress. It is conceivable that the non-microfibrillar layer that completely covers the surface of non-dried PMs of *S. sebiferum* is composed of material similar to that found on the torus surface of other species. The extreme difficulty in imaging the non-microfibrillar layer indicates the presence of soft or adhesive properties. Such properties are appropriate for a regulatory, rather than structural, role. It is easy to imagine that the role could be part of an ionically controlled hydrogel swelling mechanism proposed by Zwieniecki *et al.* (2004) to regulate water passage and air movement (Krahmer & Côté 1963). Possibly a thin, mucilaginous hydrogel could be a soft, self-sealing layer that would allow for the penetration of nanometer-sized particles into the interior of the as observed by Choat *et al.* (2003). Better images of the surface of this mucilaginous surface might increase our understanding of its properties.

A future task will be to chemically dissect the PM so that the identity of the surface structures, and their effect on transpiration, can be better understood. It seems probable that only non-dried materials will be useful to study the transpiration-related structures, while dried or partially dried materials could be used to study the events relating to embolism reduction.

#### REFERENCES

- Baker, A. A., W. Helbert, J. Sugiyama & M. J. Miles. 1997. High resolution atomic force microscopy of native Valonia cellulose I microcrystals. *J. Struct. Biol.* 318: 256–261.
- Bauch, J. & H. Berndt. 1973. Variability of the chemical composition of pit membranes in bordered pits of gymnosperms. *Wood Sci. Techn.* 7: 6–19.

- Bonner, L.D. & R.J. Thomas. 1972. The ultrastructure of intercellular passageways in vessels of yellow poplar (*Liriodendron tulipifera* L.). Part I: Vessel pitting. *Wood Sci. Techn.* 6: 196–203.
- Choat, B., M. Ball, J. Luly & J. Holtum. 2003. Pit membrane porosity and water stress-induced cavitation in four co-existing dry rainforest tree species. *Plant Physiol.* 131: 41–48.
- Cochard, H., P. Cruiziat & M.T. Tyree. 1992. Use of positive pressures to establish vulnerability curves: further support for the air-seeding hypothesis and implications for pressure-volume analysis. *Plant Physiol.* 100: 205–209.
- Côté, W.A. Jr. 1958. Electron microscope studies of pit membrane structure. *For. Prod. J.* 8: 296–301.
- Duchesne, I. & G. Daniel. 1999. The ultrastructure of wood fibre surfaces as shown by a variety of microscopical methods – a review. *Nordic Pulp and Paper Res. J.* 14: 129–139.
- Dute, R.D. & A.E. Rushing. 1987. Pit pairs with tori in the wood of *Osmanthus americanus* (Oleaceae). *IAWA Bull. n.s.* 8: 237–244.
- Dute, R.D., A.E. Rushing & J.W. Perry. 1990. Torus structure and development in species of *Daphne*. *IAWA Bull. n.s.* 11: 401–412.
- Dute, R.D., A.E. Rushing & J.D. Freeman. 1992. Survey of intervessel pit membrane structure in *Daphne* species. *IAWA Bull. n.s.* 13: 113–123.
- Frey-Wyssling, A. & H.H. Bosshard. 1959. Cytology of the ray cells in sapwood and heartwood. *Holzforschung* 14: 105–110.
- Hanley, S.J., J. Giasson, J-F. Revel & D. Gray. 1992. Atomic force microscopy of cellulose microfibrils: comparison with transmission electron microscopy. *Polymer* 33: 4639–4642.
- Heuser, J. 1981. Preparing biological samples for stereo microscopy by the quick freeze, deep etch, rotary replication technique. *Meth. Cell Biol.* 22: 97–122.
- Kirby, A.R., A.P. Gunning & V.J. Morris. 1995a. Imaging xanthan gum by atomic force microscopy. *Carbohydrate Res.* 267: 161–166.
- Kirby, A.R., A.P. Gunning & V.J. Morris. 1995b. Atomic force microscopy in food research: A new technique comes of age. *Trends in Food Sci. and Techn.* 6: 359–369.
- Kirby, A.R., A.P. Gunning, V.J. Morris & M.J. Ridout. 1995. Observation of the helical structure of the bacterial polysaccharide acetan by atomic force microscopy. *Biophys. J.* 68: 360–363.
- Kirby, A.R., A.P. Gunning, K.W. Waldron, V.J. Morris & A. Ng. 1996. Visualization of plant cell walls by atomic force microscopy. *Biophys. J.* 70: 1138–1143.
- Krahmer, R.L. & W.A. Côté. 1963. Changes in coniferous wood cells associated with heartwood formation. *Tappi* 46: 42–49.
- Kuutti, L., J. Peltonen, J. Pere & O. Teleman. 1994. Identification and surface structure of crystalline cellulose studied by atomic force microscopy. *J. Microscopy* 178: 1–6.
- Matsumura, H. & W.G. Glasser. 2000. Cellulosic nanocomposites. II. Studies by atomic force microscopy. *J. Appl. Polymer Sci.* 78: 2254–2261.
- McCann, M.C., B. Wells & K. Roberts. 1990. Direct visualization of crosslinks in the primary cell wall. *J. Cell Sci.* 96: 323–334.
- Morrow, A.C. & R.R. Dute. 1998. Development and structure of pit membranes in the rhizome of the woody fern *Botrychium dissectum*. *IAWA J.* 19: 429–441.
- Parameswaran, N. & J. Bauch. 1975. On the origin of phenolic compounds in the wood rays of *Abies alba*. *Wood Sci. Techn.* 9: 165–173.
- Pesacreta, T.C., L.C. Carlson & B.A. Triplett. 1997. Atomic force microscopy of cotton fiber cell wall surfaces in air and water: Quantitative and qualitative aspects. *Planta* 202: 435–442.
- Rief, M., F. Oesterhelt, B. Heymann & H. Gaub. 1997. Single molecule force spectroscopy on polysaccharides by atomic force microscopy. *Science* 275: 1295–1297.
- Round, A.N., A.J. MacDougall, S.G. Ring & V.J. Morris. 1997. Unexpected branching observed in pectin observed by atomic force microscopy. *Carbohydrate Res.* 303: 251–253.

- Sano, Y. & R. Nakada. 1998. Time course of the secondary deposition of incrusting materials on bordered pit membranes in *Cryptomeria japonica*. *IAWA J.* 19: 285–299.
- Sano, Y., Y. Kawakami & J. Ohtani. 1999. Variation in the structure of intertracheary pit membranes in *Abies sachalinensis*, as observed by field emission scanning electron microscopy. *IAWA J.* 20: 375–388.
- Schmid, R. & R.D. Machado. 1968. Pit membranes in hardwoods – fine structure and development. *Protoplasma* 66: 185–204.
- Shevchenko, S.M., Y.S. Yu, L.G. Akim & G.W. Bailey. 1998. Comparing surface morphology of lignin-carbohydrate complex and humic substances: AFM/OR approach. *Holzforschung* 52: 149–156.
- Thimm, J.C., D.J. Burritt, W.A. Ducker & L.D. Melton. 2000. Celery (*Apium graveolens* L.) parenchyma cell walls examined by atomic force microscopy: effect of dehydration on cellulose microfibrils. *Planta* 212: 25–32.
- Thomas, R.J. 1975. The effect of polyphenol extraction on enzyme degradation of bordered pit tori. *Wood and Fiber* 7: 207–215.
- Wheeler, E.A. 1981. Intervascular pitting in *Fraxinus americana* L. *IAWA Bull.* s.n. 2: 169–174.
- Wheeler, E.A. 1982. Ultrastructural characteristics of red maple (*Acer rubrum* L.) wood. *Wood and Fiber* 14: 43–53.
- Wheeler, E.A. & R.J. Thomas. 1981. Ultrastructural characteristics of mature wood of southern red oak (*Quercus falcata* Michx.) and white oak (*Quercus alba* L.). *Wood and Fiber* 13: 169–181.
- Zwieniecki, M.A., P.J. Melcher & N.M. Holbrook. 2004. Hydrogel control of resistance in plants. *Science* 291: 1059–1062.

VOLUME 26 (4) 2005

# iaawa journal



Published at the Nationaal Herbarium Nederland  
Leiden – The Netherlands

## **International Association of Wood Anatomists & IAWA Journal**

The *International Association of Wood Anatomists* was founded in 1931 to advance the knowledge of wood anatomy in all its aspects.

The *IAWA Journal* (ISSN 0928-1541) is published quarterly at the Nationaal Herbarium Nederland (for address, see IAWA Office below).

### ***IAWA Office***

IAWA Office, c/o Nationaal Herbarium Nederland, Universiteit Leiden branch, P.O. Box 9514, Leiden, The Netherlands (fax: 31-71-5273511 — e-mail: [eevn@euronet.nl](mailto:eevn@euronet.nl))

### ***Executive Secretary***

R. B. Miller, Forest Products Laboratory, One Gifford Pinchot Dr., Madison, WI 53726-2398, U.S.A. (fax: 1-608-231-9508 — e-mail: [rmiller1@wisc.edu](mailto:rmiller1@wisc.edu))

### ***Deputy Executive Secretary***

T. Fujii, Tama Forest Science Garden - FFPRI, Todorii 1833-81, Hachioji, Tokyo 193-0843, Japan (fax: 81-426-61-5241 — e-mail: [tfujii@ffpri.affrc.go.jp](mailto:tfujii@ffpri.affrc.go.jp))

Correspondence on IAWA Membership and IAWA Journal subscriptions should be addressed to the IAWA Office in Leiden (attention E.E. van Nieuwkoop)

---

### ***Editors IAWA Journal***

P. Baas, Nationaal Herbarium Nederland, Universiteit Leiden branch, P.O. Box 9514, 2300 RA Leiden, The Netherlands (fax: 31-71-5273511 or 31-71-5273522 — e-mail: [baas@nhn.leidenuniv.nl](mailto:baas@nhn.leidenuniv.nl))

E.E. van Nieuwkoop (desk editor), same Leiden address and fax numbers (e-mail: [eevn@euronet.nl](mailto:eevn@euronet.nl))

E.A. Wheeler, Department of Wood & Paper Science, Box 8005, North Carolina State University, Raleigh, NC 27695-8005, U.S.A. (fax: 1-919-513-3496 — e-mail: [xylem@unity.ncsu.edu](mailto:xylem@unity.ncsu.edu))

### ***Associate Editors:***

Susan A. Anagnost, Syracuse, USA  
Nigel J. Chaffey, Bath, UK  
Lloyd A. Donaldson, Rotorua, New Zealand  
Barbara L. Gartner, Corvallis, USA  
Steven Jansen, Kew, UK  
Imogen Poole, Utrecht, The Netherlands  
Ute Sass, Wageningen, The Netherlands

Laurie R. Schimleck, Athens, USA  
Uwe Schmitt, Hamburg, Germany  
John Sperry, Salt Lake City, USA  
Alex C. Wiedenhoft, Madison, USA  
Michael C. Wiemann, Madison, USA  
Thomas M. Yanosky, Reston, USA

### ***Editorial Board:***

Guillermo Angeles, Xalapa, México  
Nigel J. Chaffey, Bath, UK  
Geoff M. Downes, Hobart, Australia  
Jack B. Fisher, Miami, USA  
Minoru Fujita, Kyoto, Japan  
Ryo Funada, Fuchu-Tokyo, Japan

Steven Jansen, Kew, UK  
Yoon Soo Kim, Kwangju, South Korea  
Elisabeth A. Magel, Hamburg, Germany  
Uwe Schmitt, Hamburg, Germany  
Adya P. Singh, Rotorua, New Zealand  
Mitsuo Suzuki, Aoba, Sendai, Japan

---

**IAWA Web Page:** <http://www.iawa-web.org>

## IAWA JOURNAL

Contents	page
TH. C. PESACRETA, L. H. GROOM & T. G. RIALS	
Atomic force microscopy of the intervessel pit membrane in the stem of <i>Sapium sebiferum</i> (Euphorbiaceae) .....	397
Y. OGATA & M. FUJITA	
Z-axis calibration in optical sectioning from xylem cross sections for grain angle measurement .....	427
B. LYBBER & G. KOCH	
Lignin distribution in the tropical bamboo species <i>Gigantochloa levis</i> .....	443
CH. ZHANG, M. FUJITA & K. TAKABE	
Comparison of contact and non-contact wood fibers in some hardwoods .....	457
S. K. GÜLSOY, H. EROĞLU & N. MEREV	
Chemical and wood anatomical properties of tumorous wood in a Turkish white oak ( <i>Quercus robur</i> subsp. <i>robur</i> ) .....	469
S. R. MACHADO, C. R. MARCATI, B. LANGE DE MORRETES & V. ANGYALOSSY	
Comparative bark anatomy of root and stem in <i>Styrax camporum</i> (Styracaceae) ....	477
I. POOLE & M. MIRZALE ATAABADI	
Conifer woods of the Middle Jurassic Hojedk Formation (Kerman Basin), Central Iran .....	489
M. E. OLSON	
Commentary: Typology, homology, and homoplasy in comparative wood anatomy ..	507
Reviews .....	468, 506
Wood Anatomy News: Report from a dendrochronological fieldweek in Brazil — Inside Wood website a success — Wood anatomy symposium at 7 <sup>th</sup> European Palaeobotany-Palynology Conference in Prague — New director at the Nationaal Herbarium Nederland and retirement Dr. Pieter Baas .....	523
Association Affairs: Page charge for bulky manuscripts — New members and address changes .....	527
Instructions for preparation of manuscripts .....	528

Cover: Crystal sand in an axial parenchyma cell of *Sideroxylon puberulum* A. DC. (Sapotaceae). SEM photograph by courtesy of Frederic Lens, Laboratory of Plant Systematics, K.U. Leuven, Belgium.

ISSN 0928-1541



Fig. 36. Phase. Cell wall (W) surrounds the PM, the surface of which is composed of an extensive array of parallel and crossed MFs that are organized so that they cross each other or branch in a region that is approximately 600 nm away from the cell wall. Harvested June 5, 2002. Scale bar = 219 nm.

measured. The width of MFs ranged from 22–48 nm. When MFs were arranged in pairs, the cleft between them could be as much as 22 nm deep, indicating a minimum MF height value. The observable depth of the entire microfibrillar array on an PM was frequently in the range of 90–225 nm, but no instance showing the fractured edge of such an array was observed and so the total PM thickness was unknown. Occasionally, the centralized group of MFs had total height values of more than 500 nm.

In Figure 32 there are no coiled or reticulate MFs present near the central region of the PM. In the area where the warts are exposed, the lack of MFs makes it appear that the central MFs have been fractured away completely, indicating that the non-microfibrillar remnant has been separated from the rest of the PM. This makes it likely that the surface labeled N in Figure 32 is the inner surface of a non-microfibrillar layer that is located between the MFs and the hemispherical portion of the pit chamber wall. The frequent observation of PMs that had either exclusively non-microfibrillar or fibrillar surfaces supports the idea that these two types of layers existed independently of each other, at least in a structural sense.

#### DISCUSSION

A major contribution of the present results, in terms of the *overall* structure of the PM, is that MFs are more loosely packed in non-dried PMs than in dried PMs. It is also quite likely that these loosely packed MFs are arranged in deeper, or thicker, layers than the MFs of dried PMs, although this has not been explicitly proven here. In terms of the *details* of intervessel PM structure, the present results, which benefit from

extremely good vertical resolution and are not obscured by sputtered metals/staining, substantially increase our understanding of PM structure in that they unambiguously show the presence of a thin, non-microfibrillar coating on the surface of the PM of vessel elements in both dried and non-dried vessel elements in the outermost growth ring of *S. sebiferum*. The fact that this coating is consistently observed to have a thickness that varies within a narrow range, and that the phase characteristics of the coating are invariant (i.e. it is always phase dark) indicates that the coating is a real feature. Further support for the existence of this coating is offered here by the partial removal of the coating by the acidic peroxide treatment indicating that it is a real topographic feature that is amenable to chemical treatment.

The chemical identity of the interstitial/plaque-like coating materials on and within the PM from the outer growth ring is not known at this time. The acidic peroxide chemical treatment that we used was designed to solubilize polyphenolics. Because a reduction in the extent of coating occurred after treatment, there is reason to believe that at least some component of the coating is polyphenolic. Much of the available evidence indicates that PMs are composed of MFs and polyphenolics (Bauch & Berndt 1973; Parameswaran & Bauch 1975). However, there is some evidence that pectin may be present in tori (Thomas 1975; Sano & Nakada 1998; Morrow & Dute 1998). Given the mostly crystalline, relatively rigid nature of cellulose as opposed to the softer, non-crystalline nature of both pectin and polyphenolic materials, it is likely that there would be significant differences in the phase characteristics of these constituents within the PM. Such phase differences are clearly and consistently shown in our data. However, the available AFM literature does not offer a clear criterion for differentiating lignin from pectin. Images of pectin with the AFM by Kirby *et al.* (1995b) show a mixture of non-linear filaments and small aggregates. Lignin-carbohydrate complexes have been imaged by Shevchenko *et al.* (1998) as aggregates. Undoubtedly, a careful study using a multiplicity of extractive procedures in conjunction with AFM will allow for a clearer understanding of the distribution of pectin and lignin in PMs.

In this investigation, one of the most time-consuming and intensively studied aspects of PM structure was the variability encountered with regard to the extent of the coating on the dried PM surface. This variability may reflect the same factors that led to Bauch and Berndt's (1973) observation of variability in chemical composition between neighboring pits as analyzed with microspectrophotometry. Alternatively, slight differences in developmental events, or uneven deposition of materials as the xylem sap dries after harvesting (also see later discussion of non-dried data), might be responsible. Variation in the overall thickness of the reticulate PM layer could also have been a drying artifact or it could also have been due to the lack of a highly polarized structure in the middle lamella leading to an imprecise fracture path through the PM.

The nanometer-thick coating described here for *S. sebiferum* is not necessarily similar to encrustations observed in other species. For example, Frey-Wyssling and Bosshard (1959), Wheeler (1981), and Sano and Nakada (1998) all observed that the surface of the PM of the outermost sapwood was not encrusted, whereas the older wood was encrusted. Our observations extend the literature to indicate that the outermost sapwood in *S. sebiferum* does have some non-microfibrillar material on its surface that is referred